Received: 29 January 2024 | Revised: 22 March 2024 | Accepted: 25 March 2024

DOI: 10.1002/eqe.4126

RESEARCH ARTICLE (PREPRINT)

Analytical identification of dynamic structural models: mass matrix of an isospectral lumped mass model

Daniele Sivori | **Marco Lepidi** | **Serena Cattari**

[1]Department of Civil, Chemical and Environmental Engineering (DICCA), University of Genoa, Via Montallegro 1, 16145 Genoa, Italy

Correspondence
Daniele Sivori, Department of Civil, Chemical and Environmental Engineering (DICCA), University of Genoa, Via Montallegro 1, 16145 Genoa, Italy
Email: daniele.sivori@unige.it

Abstract

Combining the accurate physical description of high-fidelity mechanical formulations with the practical versatility of low-order discrete models is a fundamental and open-ended topic in structural dynamics. Finding a well-balanced compromise between the opposite requirements of representativeness and synthesis is a delicate and challenging task. The paper systematizes a consistent methodological strategy to identify a physics-based reduced-order model (ROM) preserving the physical accuracy of large-sized models with distributed parameters (REM), without resorting to classical techniques of dimensionality reduction. The leading idea is, first, to select a limited configurational set of representative degrees of freedom contributing significantly to the dynamic response (model reduction) and, second, to address an inverse indeterminate eigenproblem to identify the matrices governing the linear equations of undamped motion (structural identification). The physical representativeness of the identified model is guaranteed by imposing the exact coincidence of a selectable subset of natural frequencies and modes (partial isospectrality). The inverse eigenproblem is solved analytically and parametrically, since its indeterminacy can be circumvented by selecting the lumped mass matrix as the primary unknown and the stiffness matrix as a parameter (or vice versa). Therefore, explicit formulas are provided for the mass matrix of the ROM having the desired low dimension and possessing the selected partial isospectrality with the REM. Minor adjustments are also outlined to remove a posteriori unphysical effects, such as defects in the matrix symmetry, which are intrinsic consequences of the algebraic identification procedure. The direct and inverse eigenproblem solutions are explored through parametric analyses concerning a multi-story frame, by adopting a high-fidelity Finite Element model as REM and an Equivalent Frame model as ROM. Before mass matrix identification, modal analysis results indicate a general tendency of ROM to underestimate natural frequencies, with the underestimation strongly depending on the actual mass distribution of the structure. After the identification of the mass matrix and the elimination of unphysical defects, isospectrality is successfully achieved. Finally, extensions to prototypical highly massive masonry buildings are presented. The qualitative and quantitative discussion of the results under variation of the significant mechanical parameters provides useful insights to recognize the validity limits of the approximations affecting low-order models with lumped parameters.

KEYWORDS
structural identification, model updating, isospectral systems, reduced order model, equivalent frame models, masonry buildings

1 | INTRODUCTION

Structural dynamics is a constantly evolving area of scientific research gradually embracing the most recent advances in information technology and data science. Advanced virtual simulations on digital models, new smart and sustainable design concepts, rapid wireless communication and sensing techniques, reliable structural health monitoring at the building and urban scales, and consistent big data management are becoming common complements of the classic background knowledge for researchers and engineers [1,2]. Within this stimulating and rapidly evolving scenario, integrating and fusing results from physical-mathematical

formulations with the output of computational models and experimental data from dynamic measurements is becoming a necessary procedural standard. This trend is gaining substantial ground in the design and management of new and existing structures and infrastructures, a field that encompasses large monitoring networks that extend up to the urban and even national scale[3,4,5]. Specifically, the more recent research trends push forward coupling monitoring systems with digital mechanical models of structures, to improve classical data-driven methodologies for structural health monitoring[6,7,8,9,10]. This integration is characterized by a continuous feedback loop between the model and the real structure being monitored, in which the model receives continuous fluxes of digital information from sensors as inputs and should be able to reproduce in output, often in real-time[11], the system's current state and its future evolution.

Within this context, the most common choice to simulate the behavior of complex structures with high accuracy is to develop high-fidelity models, mainly recurring to Finite Element (FE) discretization schemes to solve the governing equations of motion. Although FE modeling is a powerful methodological tool that occupies a leading and irreplaceable position in structural analysis, it may become unfeasible in some modern applications due to the high computational demand. Parametric architecture and engineering design, active or semi-active strategies of vibration control, continuous structural monitoring plans, early warning systems in disaster management, and rapid structural safety assessment in post-emergency scenarios are only a few examples of high-performance applications fed by experimental data, which may require very fast (or even real-time) processing times that call for low-dimension, easily adaptive or rapidly updatable models[12,13,14,15,16,17,18]. An actual possibility is to implement parametric substructuring or other reduction techniques[19], including surrogate modeling[20]. In general, model representativeness is commonly achieved through accurate calibrations based on experimental measurements. A typical example is defining an objective function weighting spectral differences, which is minimized with iterative numerical techniques[21,22,23,24]. A reasonable alternative is to search for a synthetic but representative mechanical description, that is, a lighter (low-order) model that can still capture the essential dynamical traits of the structural system but trades simulation accuracy for computational efficiency.

Among the others, an important research area that continuously requires mathematically synthetic but physically reliable structural models is seismic engineering. For masonry buildings, to which the findings discussed in the paper are applied, Equivalent Frame (EF) modeling constitutes one of the most efficient approaches for describing the seismic response, even when they exhibit strong nonlinear behavior[25,26,27,28]. According to this modeling approach, deformations and nonlinearity are confined to a few specific portions of the structure (piers and spandrels for masonry walls, respectively analogous to the role of beams and columns for frame-like structures) which are interconnected by undeformable portions (the rigid nodes) and assembled to form a three-dimensional beam-column equivalent frame. This strategy considerably reduces the number of structural elements compared to FE models[29], and, as a consequence, the degree of freedom of the system (dofs), making the model extremely efficient in simulating the dynamic response of the structure, particularly in the nonlinear regime. Recent research in the field of structural monitoring has shown that EF models can be used as efficient digital twins to be coupled with permanent vibration monitoring systems, augmenting classical data-based Structural Health Monitoring (SHM) applications with enhanced condition assessment driven by the model's physics[30]. The use of dynamic properties identified by SHM or ambient vibration tests can efficiently address their calibration and guide the choice regarding various epistemic uncertainties, such as the deformability of diaphragms[31] and the quality of wall-to-wall connections[32]. Moreover, the EF approach may be well suited for other computationally demanding tasks in machine learning, like generating physics-based training sets for damage assessment[33,34] or defining mechanically consistent bases for physics-informed strategies[35].

However, some of the modeling assumptions inherent to the EF method can have relevant implications on the dynamics of the simulated structure[36]. For instance, the simplified mass distribution along the height of the building, in which wall masses are lumped at the floor level, can deviate significantly from the actual mass distribution of the real structure–particularly for thick walls or large interstory heights, peculiarities often encountered, for example, in monumental masonry palaces. This assumption can overestimate the importance of inertial effects, lowering the predicted natural frequency of the system. Conversely, the model's perfectly rigid nodes do not capture the actual deformability of these masonry portions and make the structure stiffer, an issue that can be exacerbated by an irregular opening layout[37,38]. The repercussions can affect, among others, the model-based inverse procedures typical of structural monitoring such as model updating and digital twinning based on experimental modal data[39,40], structural identification of mechanical parameters, and model-based damage assessment. It is well known that the uncertainty affecting the solution of second-level inverse problems, such as parameter identification, stems from the one affecting the first-level problem of modal identification, and it is usually greater [41]. In these applications, thus, the detrimental effects of modeling approximation and errors can be further amplified to an unknown extent.

Based on this motivating background, the main objective of the paper is to develop a consistent methodological strategy to identify a synthetic structural model with lumped parameters (ROM), preserving the descriptive accuracy of a reference large-sized model with distributed parameters (REM) that stands as an – ideally – perfect representation of the physical system under investigation. The candidate ROM is searched in the family of physics-based models, whose governing equations of motion are fully characterized by mechanically consistent coefficients, that is, stiffness and mass matrices. According to these leading ideas, the effective representativeness of the ROM is pursued by stating an inverse modal problem, based on imposing isospectrality, that is, by requiring that the modal properties of the ROM coincide with a significant subset of natural frequencies and modes of the REM (Section 2). According to theorems of linear algebra, the inverse modal problem is solved analytically by assuming the mass matrix of the ROM as the principal unknown and its stiffness matrix as a known parameter. The identification accuracy and the solution sensitivity are evaluated by parametric analyses, solved through numerical FE-based methods (Section 3). Indeed, a family of isospectral lumped mass EF models is identified from a known set of frequencies and modes parametrically generated by a reference distributed mass FE model. Finally, the application to prototypical case studies highlights some limitations that may occur when dealing with different typologies of existing masonry structures (Section 4). Adjustments to overcome such shortcomings by means of mass calibration are provided. Concluding remarks are finally pointed out.

2 | STRUCTURAL IDENTIFICATION OF THE MASS MATRIX

2.1 | Direct spectral problem: Modal Analysis

The structural model of a generic mechanical system, whose dynamic configuration vector $\mathbf{u}$ includes N degrees of freedom (dofs), is considered. Within the range of small oscillations and in the absence of dissipation, the free undamped response of the system is governed by a pair of real-valued $N \times N$ symmetric structural matrices, the positive-definite mass matrix $\mathbf{M}$ and the stiffness matrix $\mathbf{K}$. Given the mass and stiffness matrices (data), the classical Modal Analysis consists of determining all the spectral properties of the structural model (the unknowns), that is, the natural frequencies ω_i and normalized (unitary amplitude) modes $\boldsymbol{\psi}_i$, for $i = 1, ..., N$. From a methodological point of view, this mathematical issue can be regarded as a *Direct Spectral Problem*, requiring the statement of a linear generalized eigenproblem, reading

$$(\mathbf{K} - \lambda \mathbf{M})\, \boldsymbol{\phi} = \mathbf{0} \tag{1}$$

whose solution (*eigensolution*) consists of $M \leq N$ non-defective and generally distinct real eigenvalues $\lambda_i = \omega_i^2$, for $i = 1, ..., M$, that can be collected in the diagonal $M \times M$ matrix $\boldsymbol{\Lambda} = \text{diag}(\lambda_1, ..., \lambda_i, ..., \lambda_M)$, and the related set of real independent eigenvectors $\boldsymbol{\phi}_i = \alpha_i \boldsymbol{\psi}_i$ (where α_i is a normalization factor), that can be collected column-wise in the $N \times M$ modal matrix $\boldsymbol{\Phi} = [\boldsymbol{\phi}_1 ... \boldsymbol{\phi}_i ... \boldsymbol{\phi}_M]$. The eigensolution is said to be *complete* if $N = M$.

2.2 | Inverse spectral problem: Structural Identification

Several deterministic and non-deterministic procedures exist to establish and solve the first-level *Spectral Identification Problem*, targeted at determining the spectral properties (matrices $\boldsymbol{\Lambda}$ and $\boldsymbol{\Phi}$) of a mechanical system if its structural properties (matrices $\mathbf{M}$ and $\mathbf{K}$ and, often, the model dimension N) are unknown or uncertain. Classical techniques are based on numerical processing experimental signals of the structural free or forced response, in the frequency or time domains[42,43,44,45]. Although – in principle –spectral properties could be completely determined ($M = N$), it is relatively common to accept incomplete solutions ($M \leq N$).

Once the spectral properties (matrices $\boldsymbol{\Lambda}$ and $\boldsymbol{\Phi}$) are known from the solution of the Spectral Identification Problem, various methodologies may be employed to systematically approach the second-level *Structural Identification Problem*, targeted at determining the structural properties (matrices $\mathbf{M}$ and $\mathbf{K}$) of the mechanical system[46,47,48,49]. Recognizing the reversed role assumed by the spectral matrices $\boldsymbol{\Lambda}$ and $\boldsymbol{\Phi}$ (data) and the structural matrices $\mathbf{M}$ and $\mathbf{K}$ (unknowns) in the governing equation (1), this mathematical issue can be regarded as an *Inverse Spectral Problem*. Generally, the available information consists of an incomplete eigensolution, including the lowest M natural frequencies (eigenvalues $\boldsymbol{\Lambda}$) and the corresponding modes (eigenvectors $\boldsymbol{\Phi}$). In the absence of additional data (e.g. ortho-normalization factors[50] or modal sensitivities to known structural perturbations[51]), the unknown structural matrices cannot be determined independently of each other[52,53].

For the purpose of the present work, in the following, a parametric strategy is outlined to solve the *Structural Mass Identification Problem* of determining analytically – without approximations – the $N \times N$ mass matrix $\mathbf{M}$ (unknown) of a linear mechanical model with assigned $N \times N$ stiffness matrix $\mathbf{K}$ (parameter). The model is required to possess specific (assigned) spectral properties, that is, a known but incomplete set of frequencies and modes (data), given by the $M \times M$ eigenvalue matrix $\mathbf{\Lambda}$ and the $N \times M$ eigenvector matrix $\mathbf{\Phi}$, respectively. Naturally, the roles of the mass matrix (unknown) and the stiffness matrix (parameter) could be exchanged.

From the mathematical viewpoint, the solution of the Structural Mass Identification Problem can be based on noticing that – regardless of its completeness – the solution of the eigenproblem (1) must satisfy the fundamental relation $\mathbf{K\Phi} = \mathbf{M\Phi\Lambda}$. By transposing and invoking the symmetry properties $\mathbf{K}^\top = \mathbf{K}$, $\mathbf{M}^\top = \mathbf{M}$ and $\mathbf{\Lambda}^\top = \mathbf{\Lambda}$, the relation can be expressed more conveniently as

$$\mathbf{\Lambda\Phi}^\top\mathbf{M} = \mathbf{\Phi}^\top\mathbf{K} \tag{2}$$

which can be regarded as a *linear matrix equation*, where $\mathbf{M}$ is the matrix unknown, $\mathbf{\Lambda\Phi}^\top$ is the matrix coefficient and $\mathbf{\Phi}^\top\mathbf{K}$ is the known matrix term. It may be worth noting that the coefficient $\mathbf{\Lambda\Phi}^\top$ and the known term $\mathbf{\Phi}^\top\mathbf{K}$ are rectangular $M \times N$ matrices in the general case. According to a theorem of linear algebra[54], the conditions for the existence of a symmetric solution $\mathbf{M}$ are satisfied (see Appendix A), and the symmetric solution can be expressed as the sum

$$\mathbf{M} = \tilde{\mathbf{M}} + \hat{\mathbf{M}} + \bar{\mathbf{M}} \tag{3}$$

where three terms of the sum are individually symmetric and read

$$\tilde{\mathbf{M}} = \left(\mathbf{\Lambda\Phi}^\top\right)^\dagger \left(\mathbf{\Phi}^\top\mathbf{K}\right) + \left(\mathbf{\Phi}^\top\mathbf{K}\right)^\top \left[\left(\mathbf{\Lambda\Phi}^\top\right)^\dagger\right]^\top \tag{4}$$

$$\hat{\mathbf{M}} = -\left(\mathbf{\Lambda\Phi}^\top\right)^\dagger \left(\mathbf{\Lambda\Phi}^\top\right) \left(\mathbf{\Phi}^\top\mathbf{K}\right)^\top \left[\left(\mathbf{\Lambda\Phi}^\top\right)^\dagger\right]^\top \tag{5}$$

$$\bar{\mathbf{M}} = \left[\mathbf{I} - \left(\mathbf{\Lambda\Phi}^\top\right)^\dagger \left(\mathbf{\Lambda\Phi}^\top\right)\right] \mathbf{Z} \left[\mathbf{I} - \left(\mathbf{\Lambda\Phi}^\top\right)^\dagger \left(\mathbf{\Lambda\Phi}^\top\right)\right]^\top \tag{6}$$

where the dag indicates the Moore-Penrose pseudo-inverse (applicable to rectangular matrices), $\mathbf{I}$ is the $N \times N$ identity matrix, and $\mathbf{Z}$ is a $N \times N$ arbitrary symmetric matrix[54]. If spectral data are complete ($M = N$), the Moore-Penrose pseudo-inversion coincides with the inversion (applied to square matrices), and the last term $\bar{\mathbf{M}}$ vanishes identically. Formulations of nonnegative-definite and positive-definite solutions to Eq. (3) can be found[54,55,56], while the structural identification problem in the presence of internal resonances can be treated with perturbation methods[57].

The analytical solution (3) provides the symmetric mass matrix $\mathbf{M}$ of structural models possessing the assigned spectral properties $\mathbf{\Lambda}$ and $\mathbf{\Phi}$. The solution is independent of the eigenvector normalization, as expected. Qualitative and quantitative remarks can be pointed out to discuss the solution from the mathematical and physical viewpoints

- the identified mass matrix $\mathbf{M}$ (solution) nonlinearly depends on the spectral matrices $\mathbf{\Lambda}$ and $\mathbf{\Phi}$ (data), but is a linear function of the stiffness matrix $\mathbf{K}$ (parameter). Physically, this result states that a family of structural systems with different mass matrices, parametrized by the respective stiffness matrices, have identical spectral properties (*isospectral systems*).
- for fixed stiffness matrix $\mathbf{K}$ and incomplete spectral data ($M < N$), the identified mass matrix $\mathbf{M}$ is not unique, depending linearly on the arbitrary matrix $\mathbf{Z}$. Physically, this result states that a family branch of structural systems with the same stiffness but different mass matrices have an incomplete subset of M identical spectral properties (*M-isospectral isostiff systems*).
- incomplete spectral properties $\mathbf{\Lambda}$ and $\mathbf{\Phi}$ generate anyway complete solutions $\mathbf{M}$, with the same dimensions of the stiffness $\mathbf{K}$ and the arbitrary matrix $\mathbf{Z}$. This remark highlights that the extra $(N-M)$ frequencies and modes that complete the spectra of the identified structural system are spurious and have no physical meaning.

As a final remark, the formula (3) provides closed-form analytical solution of the structural identification problem, which profitably allows the solver to by-pass the excessive computational burden and the ill-conditioning issues often related to the numerical solution of inverse spectral problems based on the constrained minimization of an objective function describing the modal differences in the structural parameter space.

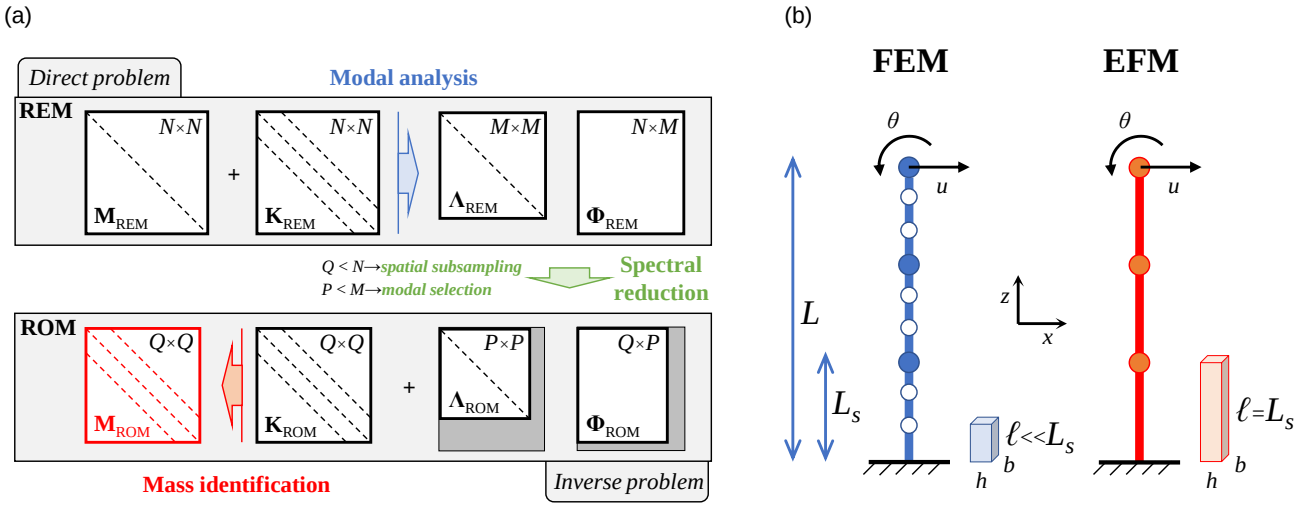

FIGURE 1 (a) Mass matrix identification of an isospectral reduced order model (ROM) starting from the known eigensolution of a reference model (REM). In this work, (b) a high-fidelity Finite Element Model (FEM) is assumed as the REM, whereas a simplified Equivalent Frame Model (EFM) constitutes the ROM.

2.3 | Reduced-Order Model Identification

Suppose the REference Model (REM) of a real dynamical system is available. REM could be, ideally, the physical system itself or, alternately, a sufficiently accurate continuous or discrete mathematical model. REM is assumed to provide a set of reference natural frequencies and modes of the system, which can be either (i) experimentally identified, if REM coincides with the physical system itself, or (ii) determined by the analytical solution of the equations governing the free undamped dynamics of a mathematical model, or finally (iii) carried out from the numerical solution of a high-fidelity computational model, as commonly happens for complex structural systems.

The primary objective of this work is the structural identification of a discrete synthetic Reduced-Order Model (ROM), describing the same dynamical system with the desired accuracy, according to a criterion of isospectrality. It is important to note that ROM is not required to descend directly from REM through reduction processes, such as substructuring or condensation. Being an accurate model by assumption, REM must be characterized by a high number of N dofs. Being synthetic by definition, ROM is postulated to be a simplified model, characterized by a lower number $Q \leq N$ of dofs. The dofs of the ROM are supposed to be a subset of the dofs of the REM (*spatial subsampling*). The key requirement is that the spectrum of ROM is included in the spectrum of the REM. In a relaxed sense, ROM and REM can be considered *isospectral systems*[58]. Indeed, strict isospectrality rigorously indicates the coincidence of all the spectral properties (frequencies and modal shapes). Relaxed isospectrality between ROM and REM here refers to the coincidence of $P \leq N$ frequencies and modes. Indeed, the number of known frequencies and modes is $M \leq N$, due to *modal truncation* (for analytical or computational REM model) or *incomplete spectral identification* (for physical REM system). Furthermore, only a subset of P of the known frequencies and modes M is selected to identify the ROM model. This process of *modal selection* can be driven by different criteria of inclusion or exclusion. Roughly, modal selection generally must include all frequencies and modes significantly contributing to a particular structural analysis (e.g. lowest frequencies and largest participating mass ratios in seismic engineering, internal subharmonic or superharmonic resonance conditions in nonlinear structural dynamics). On the contrary, modal selection must exclude modes strongly localized in the REM dofs not included in the subset of ROM dofs. The coincidence of modes, instead, is here intended as the exact collinearity of the modal subvectors composed of Q out of N dofs, as a consequence of the *spatial subsampling* of the REM.

The leading idea is to adapt the methodological strategy of structural identification presented in Section 2.2, which provides an exact solution for REM, to the identification of the unknown $Q \times Q$ mass matrix $\mathbf{M}_{\text{ROM}}$ of an isospectral ROM (Figure 1a). The strategy is based on knowledge of (i) the spectral properties of REM, consisting of M frequencies, collected in the $M \times M$

matrix $\mathbf{\Lambda}_{\mathrm{REM}}$, and modes, collected in the $N \times M$ modal matrix $\mathbf{\Phi}_{\mathrm{REM}}$, and (ii) the $Q \times Q$ stiffness matrix $\mathbf{K}_{\mathrm{ROM}}$ of the ROM, by assignment. Therefore, relaxed isospectrality is imposed by assigning the spectral properties of the ROM, by – first – selecting P out of M frequencies of the REM to define the $P \times P$ matrix $\mathbf{\Lambda}_{\mathrm{ROM}}$, and – second – selecting P out of M modes of the REM, properly subsampled to define the $Q \times P$ matrix $\mathbf{\Phi}_{\mathrm{ROM}}$. Therefore, the mass matrix $\mathbf{M}_{\mathrm{ROM}}$ is identified by specifying Eq. (3) according to the formula

$$\mathbf{M}_{\mathrm{ROM}} = \tilde{\mathbf{M}}_{\mathrm{ROM}} + \hat{\mathbf{M}}_{\mathrm{ROM}} + \bar{\mathbf{M}}_{\mathrm{ROM}} \tag{7}$$

where three terms of the sum read

$$\begin{aligned}
\tilde{\mathbf{M}}_{\mathrm{ROM}} &= \left(\mathbf{\Lambda}_{\mathrm{ROM}}\mathbf{\Phi}_{\mathrm{ROM}}^{\top}\right)^{\dagger}\left(\mathbf{\Phi}_{\mathrm{ROM}}^{\top}\mathbf{K}_{\mathrm{ROM}}\right) + \left(\mathbf{\Phi}_{\mathrm{ROM}}^{\top}\mathbf{K}_{\mathrm{ROM}}\right)^{\top}\left[\left(\mathbf{\Lambda}_{\mathrm{ROM}}\mathbf{\Phi}_{\mathrm{ROM}}^{\top}\right)^{\dagger}\right]^{\top} \\
\hat{\mathbf{M}}_{\mathrm{ROM}} &= -\left(\mathbf{\Lambda}_{\mathrm{ROM}}\mathbf{\Phi}_{\mathrm{ROM}}^{\top}\right)^{\dagger}\left(\mathbf{\Lambda}_{\mathrm{ROM}}\mathbf{\Phi}_{\mathrm{ROM}}^{\top}\right)\left(\mathbf{\Phi}_{\mathrm{ROM}}^{\top}\mathbf{K}_{\mathrm{ROM}}\right)^{\top}\left[\left(\mathbf{\Lambda}_{\mathrm{ROM}}\mathbf{\Phi}_{\mathrm{ROM}}^{\top}\right)^{\dagger}\right]^{\top} \\
\bar{\mathbf{M}}_{\mathrm{ROM}} &= \left[\mathbf{I} - \left(\mathbf{\Lambda}_{\mathrm{ROM}}\mathbf{\Phi}_{\mathrm{ROM}}^{\top}\right)^{\dagger}\left(\mathbf{\Lambda}_{\mathrm{ROM}}\mathbf{\Phi}_{\mathrm{ROM}}^{\top}\right)\right]\mathbf{Z}\left[\mathbf{I} - \left(\mathbf{\Lambda}_{\mathrm{ROM}}\mathbf{\Phi}_{\mathrm{ROM}}^{\top}\right)^{\dagger}\left(\mathbf{\Lambda}_{\mathrm{ROM}}\mathbf{\Phi}_{\mathrm{ROM}}^{\top}\right)\right]^{\top}
\end{aligned} \tag{8}$$

where here $\mathbf{I}$ stands for the $Q \times Q$ identity matrix and $\mathbf{Z}$ indicates a $Q \times Q$ arbitrary symmetric matrix. It may be worth noting that the symmetry of the mass matrix $\mathbf{M}_{\mathrm{ROM}}$ cannot be taken for granted a priori, because the term $\hat{\mathbf{M}}_{\mathrm{ROM}}$ is not symmetric in the general case (whereas the other terms $\tilde{\mathbf{M}}_{\mathrm{ROM}}$ and $\bar{\mathbf{M}}_{\mathrm{ROM}}$ are symmetric by construction). The defect of symmetry in the term $\hat{\mathbf{M}}_{\mathrm{ROM}}$ is an unavoidable consequence of the required isospectrality. Indeed, the spectral properties $\mathbf{\Lambda}_{\mathrm{ROM}}$ and $\mathbf{\Phi}_{\mathrm{ROM}}$ are requested to belong to the eigensolution space of the stiffness matrix $\mathbf{K}_{\mathrm{ROM}}$ *with respect to* the unknown mass matrix $\mathbf{M}_{\mathrm{ROM}}$ (and do not belong to eigensolution space of the known stiffness matrix $\mathbf{K}_{\mathrm{ROM}}$). Moreover, the structural symmetry of the term $\bar{\mathbf{M}}_{\mathrm{ROM}}$ prevents using the arbitrary matrix $\mathbf{Z}$ to compensate for the symmetry defect.

The structural identification of the ROM isospectral to the REM is complete with the mass matrix determined according to Eq. (7). Naturally, the role of the ROM stiffness matrix $\mathbf{K}_{\mathrm{ROM}}$ (assigned parameter) and the ROM mass matrix $\mathbf{M}_{\mathrm{ROM}}$ (unknown) can be exchanged, with a few algorithmic adjustments of a minor methodological value[59]. Anyway, the final purpose is to achieve all the structural properties of a ROM that is both synthetic and representative. Representativeness is guaranteed by isospectrality, while synthesis can be pursued by enforcing low-dimensionality (e.g. by setting $P \ll N$) and shape simplicity of the assigned stiffness matrix $\mathbf{K}_{\mathrm{ROM}}$ (e.g. by requiring $\mathbf{K}_{\mathrm{ROM}}$ to be a banded matrix). It may be worth noting that the reference structural matrices $\mathbf{M}_{\mathrm{REM}}$ and $\mathbf{K}_{\mathrm{REM}}$ are not involved in the identification procedure, so the identifier does not have particular constraints in defining REM (mathematically or experimentally), provided that the accuracy of the model is sufficient to provide the necessary spectral information $\mathbf{\Lambda}_{\mathrm{REM}}$ and $\mathbf{\Phi}_{\mathrm{REM}}$, from which the data $\mathbf{\Lambda}_{\mathrm{ROM}}$ and $\mathbf{\Phi}_{\mathrm{ROM}}$ must be selected and subsampled. In the following Section, this problem is attacked by adopting a high-fidelity Finite Element Model (FEM) as REM, and a simplified Equivalent Frame Model (EFM) as ROM (Figure 1b).

3 | PARAMETRIC ANALYSIS

This section presents a testbed of relevant physical interest aimed at the identification of an isospectral EFM of a real civil structure. The EFM, commonly employed to simulate the seismic response of masonry buildings, describes the (ideally) continuous distribution of wall masses along the elevation as a discrete ensemble of masses lumped at the floor levels. It is of primary interest, for this reason, to focus the general inverse procedure developed in Section 2.2 on the identification of an isospectral mass matrix for EFM. This task is carried out on a benchmark case study, a model sufficiently elaborated to allow the execution of parametric and convergence analyses and simple enough to be governed by a few mechanical parameters.

The mechanical model under investigation is a simplified but realistic representation of an actual civil structure developing in height, i.e. a multi-story building exhibiting a nondissipative elastic behavior at low oscillation amplitudes. The physical system is characterized by the continuous interstory distribution of mass and stiffness provided by the vertical structural elements (reinforced concrete columns, masonry piers, etc.) and, at the floor level, by the additional mass given by horizontal elements (floor beams and diaphragms, vaults, etc.).

The structure is idealized by a vertical cantilever beam of length L oscillating transversally in the plane, with constant cross-sectional properties along its length and a certain number of added point masses at the floor levels. The REM and ROM discretizations follow two alternative approaches (Figure 1b) that differ in mesh refinement but share the same constitutive finite

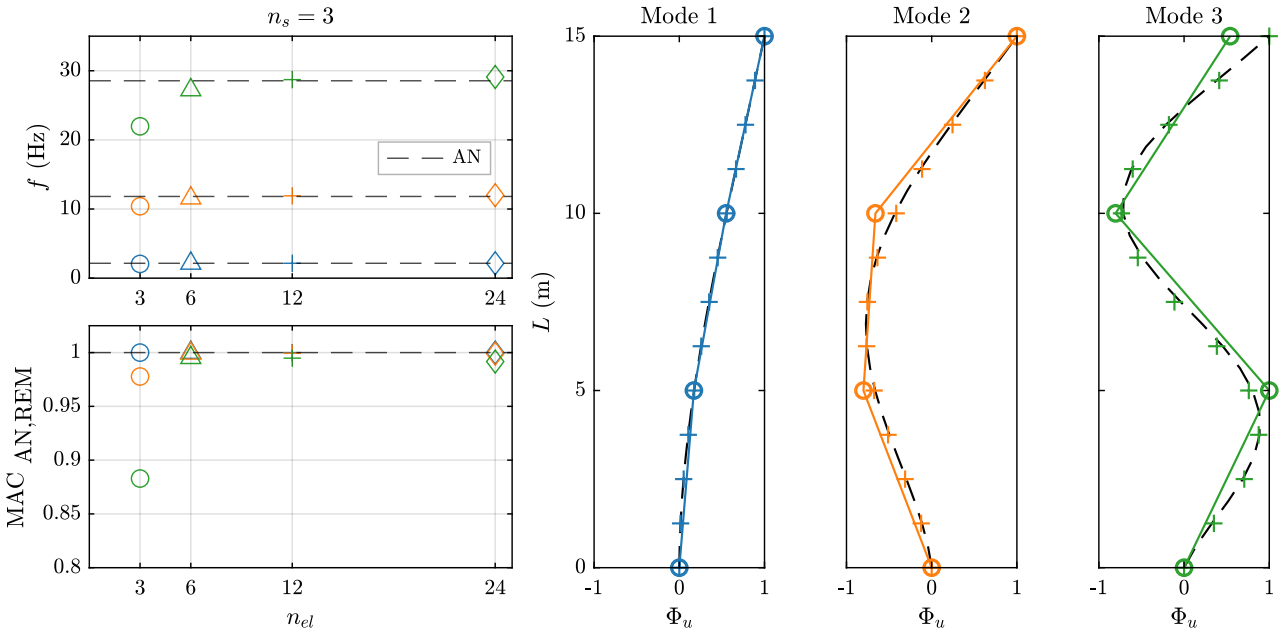

FIGURE 2 Convergence of REM to the analytical eigensolution of a continuous Timoshenko beam with no added masses (parameters $n_s = 3$, $L_s = 4\,\text{m}$, $b = 1\,\text{m}$, $h = 3\,\text{m}$, $E = 3000\,\text{MPa}$, $\nu = 0.5$, $\rho = 2200\,\text{kg m}^{-3}$, $q = 4000\,\text{N m}^{-2}$, see Section 3.1) for subsequent mesh refinements, i.e. increasing the total number of sub-elements n_{el}.

element, a two–nodes Timoshenko planar beam with two nodal degrees of freedom at each node, transversal displacement u and rotation θ. The element stiffness and mass matrices are reported in Appendix B.

REM model is a high-fidelity FEM that reproduces the modal properties of the physical structure with the desired precision (left of Figure 1b). The refined mesh is composed of 4 finite elements per story. Comparing REM with the analytical solution of a vibrating Timoshenko beam (with no additional masses at the floor level), this discretization grants a relative error in estimating the first three natural frequencies lower than 1 % and achieves an almost perfect correlation between mode shapes, with MAC values[60] very close to unity (see Figure 2). In this case, the length ℓ of the finite elements is much smaller than the interstory length L_s, i.e. $\ell << L_s$. Conversely, ROM is a simplified model that, according to EFM idealization, has a single finite element for each story (right of Figure 1b) and lumps both the wall and story masses at the floor nodes. In this case, the length of the finite element coincides with the interstory length, i.e. $\ell = L_s$.

3.1 | Parametrization

REM and ROM models are parametrized by the number of floors n_s and a set of mechanical parameters that vary independently from each other. The independent dimensional parameters and their assumed range of variation are reported at the top of Table 1. From a structural point of view, n_s distinguishes single-story buildings from multi-story buildings and, in general, low-rise from high-rise structures. The other mechanical parameters define the geometrical properties of the beam cross-section, the elastic property of the constitutive materials, and the beam and floor masses. By defining the interstory length L_s, the total length of the beam is $L = L_s n_s$. The beam cross-section is rectangular with height b and width h. The material is isotropic and characterized by Young's modulus of elasticity E and Poisson coefficient ν – which univocally determine the shear modulus G, see Appendix B – with mass density ρ. Finally, the parameter q accounts for the typical self weight per unit area of different types of horizontal diaphragms, ranging from light timber floors to heavy reinforced concrete floors or masonry vaults.

The dependent dimensional parameters are reported at the bottom of Table 1. The total floor mass m_f is the result of the floor load q acting on the area of influence at the top of the beam, assuming an influence width of 2.5 m. The total mass between floors, the mass between floors m_s, instead corresponds to the mass of the sole beam.

TABLE 1 Independent and dependent dimensional parameters of the oscillating beam and their assumed range of variation.

Parameter	Description	Units	Range
L_s	interstory length	m	2–6
b	cross-section width	m	0.4–1
h	cross-section height	m	2–6
E	Young modulus	MPa	1000–3000
ν	Poisson coefficient	-	0–0.5
ρ	mass density	kg m^{-3}	1600–2200
q	floor load	kN m^{-2}	0–8
$m_f = 2.5qh/g$	floor mass	kg	0–12 236.6
$m_s = bh\rho L_s$	interstory mass	kg	2560–79 200

TABLE 2 Nondimensional mass and slenderness parameters.

Parameter	Description	Units	Range
η	floor-to-interstory mass ratio	-	0–1.5
δ	lateral slenderness parameter	-	1–10

A minimum set of nondimensional parameters useful to synthetically describe the system is defined by

$$\eta = \frac{m_f}{m_s}, \quad \delta = \frac{L_s}{r} \tag{9}$$

where η is the floor-to-interstory mass ratio and δ accounts for the beam lateral slenderness, while $r^2 = I_x/A$ is the (square of) radius of gyration of the cross-section. This expedient effectively reduces the analysis space to only two prevalent dimensions. Both parameters assume only positive values, and for η tending to infinity, that is, when the floor mass tends to zero, the REM and ROM mass discretizations coincide with each other. Parametric analyses are carried out by exploring the parameter space through Monte Carlo sampling, assuming a uniform distribution of the dimensional parameters and a possible range of variation according to Table 1. The ranges of nondimensional parameters explored in the analyses, which are representative of the majority of practical cases, are reported in Table 2.

3.2 | Modal analysis

The agreement between the ROM and the reference REM is investigated in the framework of the direct eigenproblem for both natural frequencies and mode shapes, focusing initially on models with three interstories, i.e. $n_s = 3$. The modal distance between the models is quantified by the relative frequency difference with respect to REM $\Delta f_{\text{REM,ROM}} = (f_{\text{ROM}} - f_{\text{REM}})/f_{\text{REM}}$ and is reported for the three lowest frequency modes. The correlation between mode shapes is estimated by the well-known MAC indicator[60]. As an alternative, other criteria combining and weighting frequency differences and modal assurance measures could be employed to assess the performance of the updating procedure with a single synthetic index[21]. Figure 3 reports the results of 5000 Monte Carlo simulations in terms of frequency differences and MACs in the plane $\eta - \delta$, which form curved surfaces confirming the unique dependence on these two parameters.

The results highlight that ROM generally tends to underestimate the (reference) natural frequencies of REM, with errors becoming larger for higher-frequency modes. This difference (Figure 4a) is governed by the floor-to-interstory mass ratio η (Figure 4c), while variations in the lateral slenderness δ appear to be secondary (Figure 4e). In particular, the lower the η ratio, the higher the frequency difference – which, in the limit case $\eta = 0$ corresponding to a null floor mass, is already greater than 10 % for the second mode. The agreement between the mode shapes (Figure 4b) is acceptable, with MACs higher than 0.8, a value that is commonly considered the lower threshold for MAC acceptance. As in the previous case, low η ratios have a detrimental effect (Figure 4d). The lower the mass ratio, the worse the mode shape correlation, with MAC values quickly approaching the lower acceptance limit for higher modes. Lateral slenderness has a relevant effect on this aspect, in which the

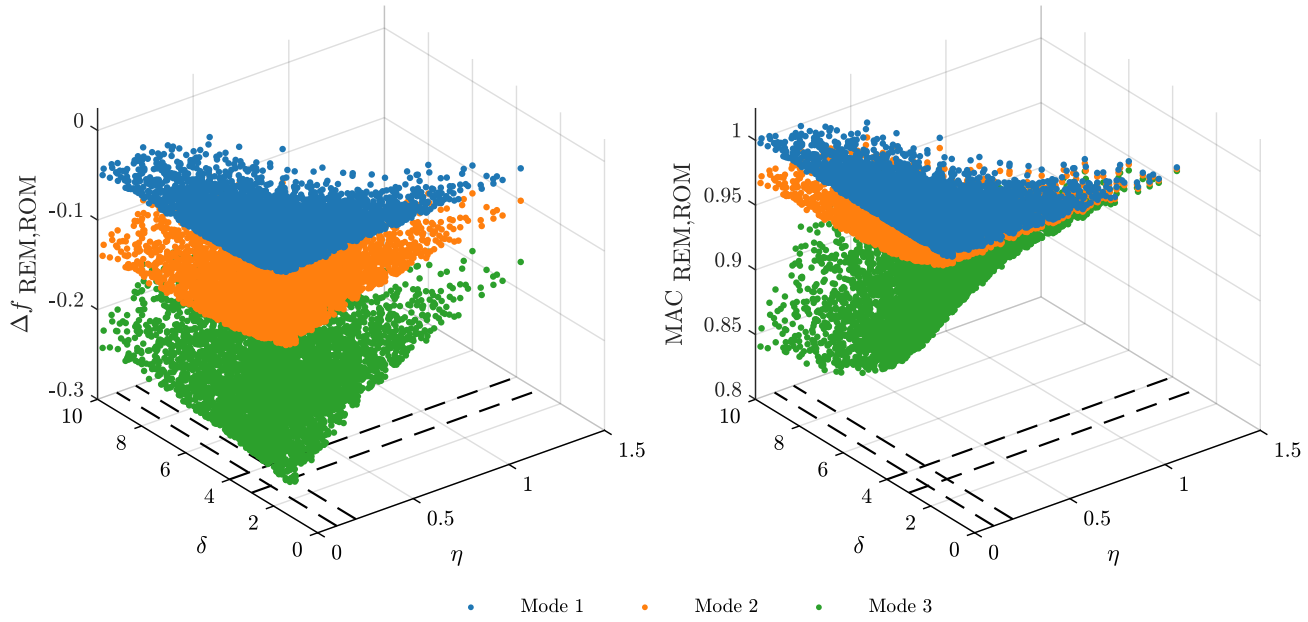

FIGURE 3 Solution of the direct problem (modal analysis) for $n_s = 3$. Comparison between REM and ROM models in terms of relative difference in natural frequency Δf and mode shape correlation index MAC, as a function of the floor-to-interstory mass ratio η and lateral slenderness parameter δ.

underestimation of higher-mode frequencies increases significantly for slender beams (Figure 4f). The influence of the floor-to-interstory mass ratio (Figure 3 and Figure 4) on the quality of the EFM approximation provided by ROM can be easily understood considering that, in two extreme cases (i) when all the mass is concentrated at the floor level, i.e. the interstory mass tends to zero and η grows to infinity, the EF model is exactly reproducing the actual mass distribution of the reference structure, whereas (ii) when all the mass is distributed at the interstory level, i.e. the floor mass tends to zero as η does, the EF model is grossly overestimating the inertia of the beam (since the distributed mass of the interstory is entirely lumped at the floor level).

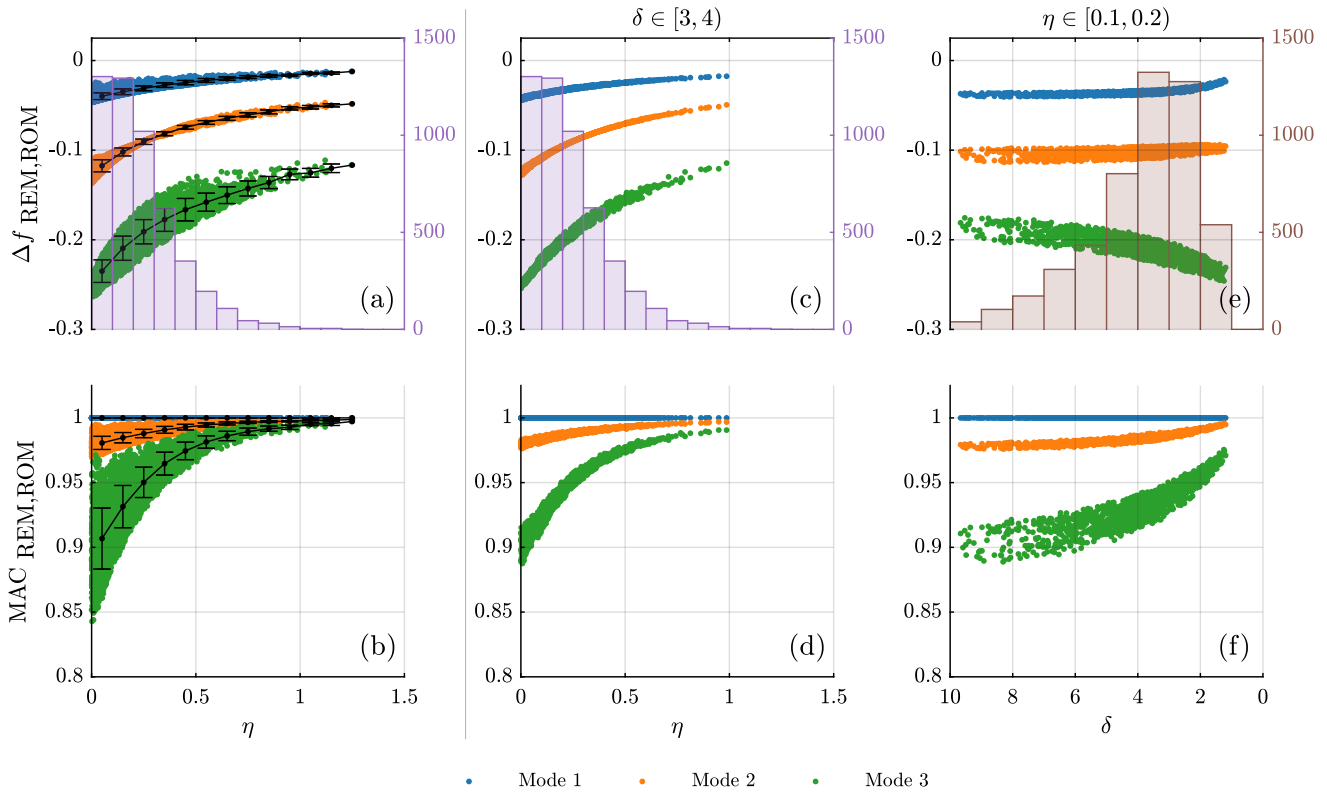

FIGURE 4 Solution of the direct problem (modal analysis) for $n_s = 3$. Comparison between REM and ROM models in terms of (a) relative difference in natural frequency Δf and (b) mode shape correlation index MAC, as a function of the floor-to-interstory mass ratio η. The observed variance is due (c,d and e,f) to the variation in the lateral slenderness parameter δ.

3.3 | Mass matrix identification

The previous analyses highlight how the EF approach can lead to a general underestimation of natural frequencies, in particular when the mass of walls prevails over the floor mass, more significantly for higher-frequency modes than for lower-order ones. This section leverages the inverse mass identification procedure theoretically developed in Section 2.2 and implemented in Section 2.3 to identify, in a loose sense, a ROM model isospectral with the REM model.

Figure 5 shows a simple explanatory example for a three-story system, i.e. $n_s = 3$. The REM system (Figure 5a), by construction, is composed of a $N \times N$ symmetric stiffness matrix $\mathbf{K}_{\text{REM}}$ and an $N \times N$ diagonal mass matrix $\mathbf{M}_{\text{REM}}$, with $N = 12$ (four beams per story). Rotational dofs have no associated mass (see Appendix B) and, thus, are condensed statically and omitted from the problem formulation without altering the original solution. This expedient effectively removes the singularity of the mass matrix, which would be deleterious for the identification. Further details are reported in Appendix C.

The ROM model (Figure 5b), according to the EF approach, is composed of just one beam per story. The system has thus dimensions $Q = 3$. As already shown by direct simulations (Section 3.2), ROM tends to underestimate the natural frequencies of REM (orange line in Figure 5b) with a direct relationship with frequency – the higher the REM frequency mode, the higher the underestimation and the relative frequency error.

An isospectral ROM* model is identified by selecting a number of modes equal to the ROM dimension, that is $P = Q = 3$, in particular the first P modes from the M modes set of REM, appropriately sampled in common dofs (see Section 2.3). The identified mass matrix $\mathbf{M}^*_{\text{ROM}}$ (Figure 5c) is quasi-symmetric and generally non-diagonal, with off-diagonal terms representing inertial couplings within the system. The identified model satisfies the relaxed modal isospectrality criteria defined in Section 2.3, with relative errors in frequency comparable to the machine precision and, practically, unitary MAC indicators.

Indeed, employing the general form of the identified mass matrix in finite element codes is not so straightforward. Either for research or commercial use, these codes commonly assume a diagonal mass matrix, a choice that grants certain advantages in

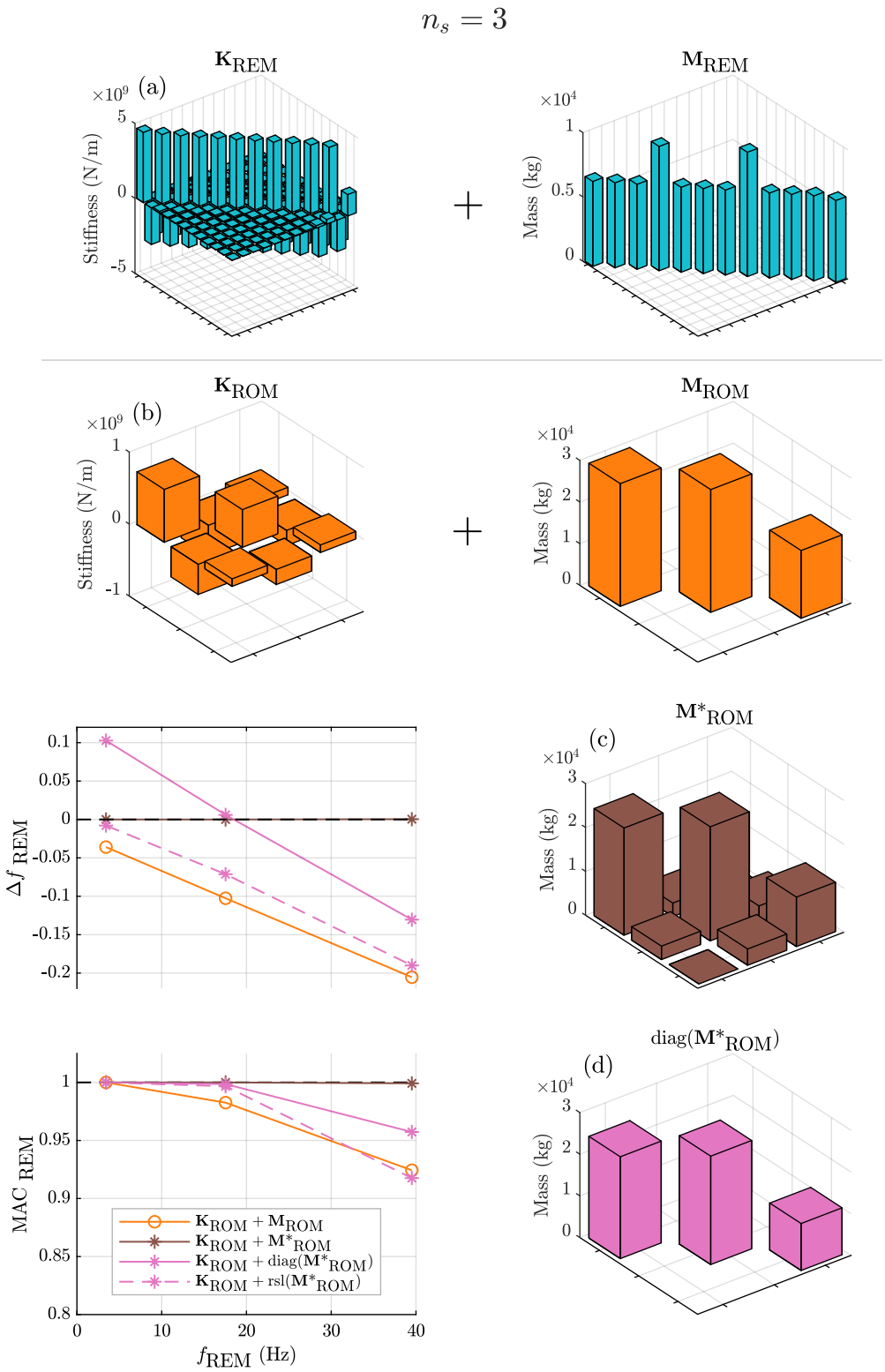

FIGURE 5 Identified mass matrix $\mathbf{M}^*$ for an isospectral ROM (parameters $n_s = 3$, $L_s = 4\,\mathrm{m}$, $b = 1\,\mathrm{m}$, $h = 3\,\mathrm{m}$, $E = 3000\,\mathrm{MPa}$, $\nu = 0.5$, $\rho = 2200\,\mathrm{kg\,m^{-3}}$, $q = 4000\,\mathrm{N\,m^{-2}}$, see Section 3.1). Spectral matrices for (a) REM and (b) ROM. (c) General form of the identified mass matrix and (d) closest diagonalized form. On the left, results in terms of relative frequency differences Δf and MAC values with respect to REM.

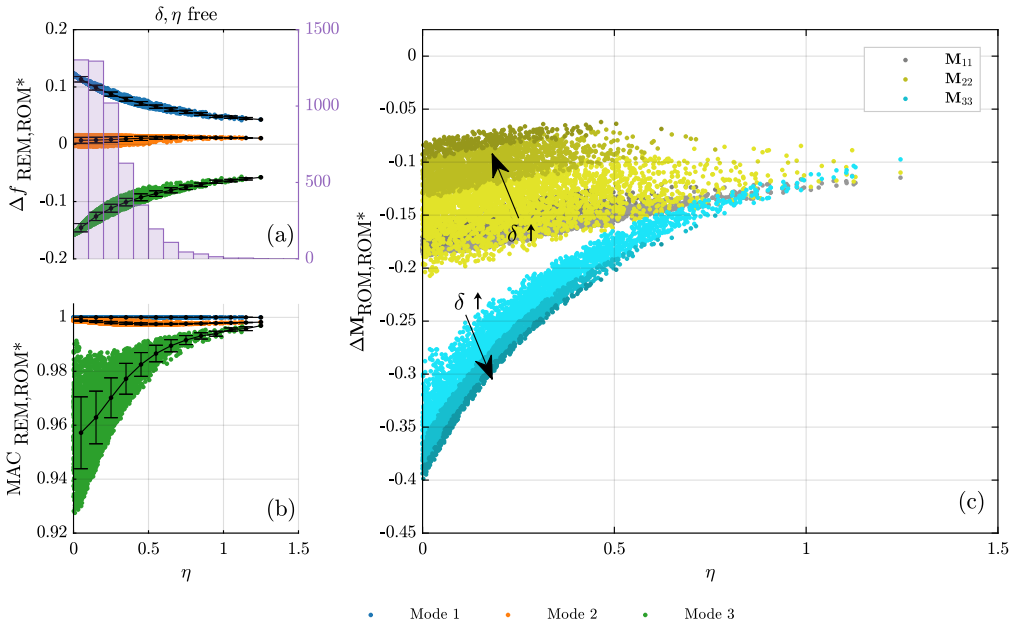

FIGURE 6 Solution of the inverse problem (mass identification) for $n_s = 3$. Comparison between REM and identified ROM (a) in terms of relative difference in natural frequency Δf and (b) mode shape correlation index MAC, as a function of the floor-to-interstory mass ratio η. The (c) variations in the mass matrix are reported, for each dofs, in terms of relative difference with respect to the original translational mass.

memory management and computational efficiency at the expense of loss of accuracy in the eigensolution. In this respect, it is worth exploring other diagonalized solutions. Adopting the Frobenius norm as a distance metric, the closest diagonal mass matrix is just its diagonal part, that is diag $(\mathbf{M}^*_{\text{ROM}})$. The mass-diagonalized identified model (Figure 5d) appears to minimize, in a least-square sense, the sum of the relative frequency differences for all the modes, improving the correlation between the mode shapes as well. In the following, this model will be referred to as *diagonalized*.

It is worth remarking that other algorithmic choices could be made to recover a diagonal mass matrix. Another well-known diagonalization technique is the row-sum lumping (rsl$(\mathbf{M}^*_{\text{ROM}})$ in Figure 5), which has the advantage of keeping unchanged the total mass of the identified model. This operation significantly improves the agreement in frequency for the fundamental mode of oscillation of the beam, the first flexural mode which usually develops as the lowest-frequency mode in three-dimensional buildings too. For this reason, this updating strategy will be adopted in the analysis of pseudo-experimental case studies (Section 4).

These aspects are further investigated by applying the mass identification procedure to the Montecarlo simulations already solved in the direct problem (Section 3.2). The focus is put on assessing the differences in the translational masses between the identified ROM mass matrix in its diagonalized form diag $(\mathbf{M}^*_{\text{ROM}})$ and the original mass matrix $\mathbf{M}_{\text{ROM}}$. Figure 6a,b shows the results of the comparison in terms of relative frequency differences and MAC values with respect to REM, respectively. Figure 6c assesses the results of the mass matrix identification by comparing the identified masses with the original ones. The alteration between the original translational mass and identified mass is estimated by the relative mass variation $\Delta M_{ii}^{\text{ROM,ROM}^*} = (M_{ii}^{\text{ROM}^*} - M_{ii}^{\text{ROM}})/M_{ii}^{\text{ROM}}$ for all the diagonal entries. This quantity effectively corresponds, in relative terms, to the variation to be applied to the ROM masses lumped at the floor level to obtain the identified model. The results show that, generally, the masses of all the floors need to be reduced – being the stiffness unchanged, this is in accordance with the underestimation of natural frequency previously highlighted. Particularly, the masses of the last floor are those that should undergo the biggest change, with relative variation ranging from –10 % for $\eta = 1$ down to –40 % in the limit case $\eta = 0$. The first and middle floor masses are less affected, with variation in the range –10 % to –20 % depending also on δ. More detailed results are reported in Table 3, which also includes the cases of one- and two-story systems.

TABLE 3 Solution of direct problem and mass identification for n_s ranging from one to three stories.

		REM, ROM					REM, ROM*							
η	n_s	$\overline{\Delta f}_1$	$\overline{\Delta f}_2$	$\overline{\Delta f}_3$	$\overline{\text{MAC}}_2$	$\overline{\text{MAC}}_3$	$\overline{\Delta \text{M}}_{11}$	$\overline{\Delta \text{M}}_{22}$	$\overline{\Delta \text{M}}_{33}$	$\overline{\Delta f}_1$	$\overline{\Delta f}_2$	$\overline{\Delta f}_3$	$\overline{\text{MAC}}_2$	$\overline{\text{MAC}}_3$
0.05	1	-0.196					-0.352			0				
	2	-0.074	-0.209		0.942		-0.151	-0.329		0.100	-0.117		0.987	
	3	-0.038	-0.112	-0.225	0.981	0.912	-0.176	-0.129	-0.334	0.113	0.007	-0.146	0.999	0.957
0.15	1	-0.166					-0.304			0				
	2	-0.064	-0.180		0.955		-0.143	-0.282		0.084	-0.097		0.985	
	3	-0.033	-0.097	-0.201	0.985	0.937	-0.168	-0.124	-0.286	0.099	0.007	-0.126	0.998	0.963
0.25	1	-0.143					-0.265			0				
	2	-0.056	-0.160		0.965		-0.137	-0.247		0.073	-0.083		0.986	
	3	-0.030	-0.086	-0.183	0.988	0.955	-0.161	-0.121	-0.250	0.088	0.008	-0.112	0.998	0.970
0.35	1	-0.123					-0.231			0				
	2	-0.049	-0.145		0.975		-0.134	-0.216		0.064	-0.072		0.988	
	3	-0.026	-0.078	-0.170	0.991	0.969	-0.155	-0.121	-0.219	0.079	0.009	-0.101	0.998	0.977
0.45	1	-0.108					-0.203			0				
	2	-0.043	-0.133		0.981		-0.130	-0.192		0.057	-0.063		0.990	
	3	-0.023	-0.071	-0.159	0.993	0.978	-0.150	-0.120	-0.194	0.071	0.010	-0.093	0.998	0.983
0.55	1	-0.095					-0.180			0				
	2	-0.039	-0.124		0.986		-0.128	-0.172		0.051	-0.057		0.991	
	3	-0.021	-0.066	-0.151	0.995	0.984	-0.145	-0.121	-0.174	0.066	0.011	-0.086	0.998	0.987
0.65	1	-0.085					-0.162			0				
	2	-0.035	-0.116		0.989		-0.125	-0.155		0.047	-0.052		0.993	
	3	-0.019	-0.062	-0.144	0.996	0.989	-0.140	-0.120	-0.157	0.061	0.012	-0.080	0.998	0.989
0.75	1	-0.077					-0.147			0				
	2	-0.032	-0.109		0.992		-0.122	-0.142		0.043	-0.047		0.994	
	3	-0.018	-0.058	-0.137	0.996	0.991	-0.135	-0.117	-0.143	0.056	0.012	-0.075	0.998	0.992
0.85	1	-0.070					-0.135			0				
	2	-0.029	-0.103		0.993		-0.118	-0.131		0.040	-0.044		0.995	
	3	-0.016	-0.055	-0.130	0.997	0.993	-0.131	-0.115	-0.132	0.053	0.012	-0.071	0.998	0.993
0.95	1	-0.066					-0.128			0				
	2	-0.028	-0.096		0.994		-0.111	-0.122		0.037	-0.040		0.995	
	3	-0.016	-0.051	-0.122	0.997	0.994	-0.124	-0.107	-0.123	0.049	0.011	-0.065	0.998	0.994
1.05	1	-0.058					-0.113			0				
	2	-0.024	-0.094		0.996		-0.113	-0.111		0.036	-0.038		0.996	
	3	-0.014	-0.050	-0.120	0.998	0.996	-0.122	-0.112	-0.112	0.047	0.011	-0.063	0.998	0.995
1.15	1	-0.056					-0.109			0				
	2	-0.023	-0.090		0.996		-0.109	-0.107		0.034	-0.036		0.996	
	3	-0.013	-0.048	-0.115	0.998	0.997	-0.118	-0.107	-0.108	0.045	0.011	-0.060	0.998	0.996
1.25	1	-0.049					-0.096			0				
	2	-0.020	-0.087		0.998		-0.108	-0.097		0.033	-0.035		0.997	
	3	-0.012	-0.046	-0.111	0.999	0.998	-0.115	-0.110	-0.097	0.043	0.011	-0.058	0.998	0.997

TABLE 4 Example cases of residential buildings and monumental palaces built with masonry, with a different number of stories, light or heavy foors. Material properties are shared among all the examples ($E = 2500$ MPa, $\nu = 0.5$, $\rho = 2100$ kg m^{-3}).

Case	Description	n_s	b (m)	h (m)	L_s (m)	q (kN m^{-2})	η	δ
a	Low-rise building with light floors	2	0.5				0.162	
b	Mid-rise building with light floors	4	0.65	3	3	2	0.124	3.464
c	High-rise building with light floors	6	0.8				0.101	
d	Low-rise building with heavy floors	2	0.5				0.405	
e	Mid-rise building with heavy floors	4	0.65	3	3	5	0.311	3.464
f	High-rise building with heavy floors	6	0.8				0.253	
g	Mid-rise palace with light floors	4	0.8	4	5	2	0.061	4.330
h	High-rise palace with light floors	6	1				0.049	
i	Mid-rise palace with heavy floors	4	0.8	4	5	5	0.182	4.330
j	High-rise palace with heavy floors	6	1				0.146	

4 | APPLICATION TO PROTOTYPICAL MASONRY STRUCTURES

The previous section provided a general overview of the modal behavior of a lumped mass ROM when simulating a distributed mass REM, highlighting its tendency to underestimate natural frequencies and proposing a mass-matrix identification strategy to improve its spectral properties. The purpose of this section is to address in detail some practical cases that are often encountered in the modeling of existing or new structures, focusing in particular on masonry buildings. For the seismic analysis of this class of structures, in fact, a ROM approach such as the EFM (Section 3.3) is often adopted to keep a low computational burden, even for accurate nonlinear dynamic analyses. In particular, the following analysis employs numerical results generated by REM for prototypical cases as pseudo-experimental modal data for the ROM identification procedure.

It is interesting, first, to assess the value of the adimensional parameters that govern the ROM direct problem in common cases. Second, solving the identification procedure with the proper mass diagonalization strategy can provide useful indications regarding model updating, in particular for all those cases in which the model dynamics plays a fundamental role and requires an accurate model calibration. That is, for example, to properly capture structural resonance with the seismic input, or to employ the modal properties of the model as a proxy for damage in model-driven structural health monitoring [17].

The examples analyzed represent typical structural configurations of existing masonry buildings, either residential buildings or historical palaces, low- (two stories), mid- (four stories), or high-rise (six stories), with homogeneous geometrical and material properties along the height – except for wall thickness which, according to common construction rules, is decreasing with increasing height. The structures are modeled as rigidly connected to the ground, i.e., assuming a fixed-base condition (Section 3.1) and no soil-structure interaction. Two different typologies of flooring systems are considered, which differ in terms of their mass contribution to the floor level. The first type, light floor, is representative of light horizontal diaphragms which can be encountered in historical buildings, such as timber floors. The second type, heavy floor, accounts for the presence of heavier reinforced concrete floors or masonry vaults. Indeed, in order to keep the analysis and its results as general as possible, the simulation does not capture other structural specificities (such as the story variability in height, or the possible presence of different types of diaphragms).

Table 4 reports, for the made-up examples, the dimensional parameters and resulting adimensional parameters μ and δ that govern the direct problem for ROM. It is clear how the floor-to-story mass ratio increases primarily moving from light to heavy floors and, secondarily, in low-rise buildings compared to high-rise (due to thinner walls). The limited variation of the slenderness parameter δ depends on the cross-sectional geometry of masonry piers.

Table 5 reports the solution of modal analysis for ROM compared to the reference natural frequency of REM. Here, the mass identification procedure follows the row-sum diagonalization (see Section 3.3) focusing on improving the agreement of the first or fundamental natural frequency. This choice goes in the direction of giving practical indications regarding the calibration of fundamental flexural modes in actual three-dimensional models of structures [36,31,61,32]. These modes develop at low frequencies provided a certain rigidity of diaphragms, are usually the easiest to excite (for example, by base accelerations) and, thus, have a great impact on the dynamic response. The results, as already shown by Montecarlo simulations (Section 3.3),

TABLE 5 Mass identification for the example cases reported in Table 4. The procedure adopts a first-mode oriented optimization (row-sum method, Section 3.3).

	ROM	ROM*							
Case	Δf_1^{REM}	ΔM_{11}^{ROM}	ΔM_{22}^{ROM}	ΔM_{33}^{ROM}	ΔM_{44}^{ROM}	ΔM_{55}^{ROM}	ΔM_{66}^{ROM}	ΔM_{tot}^{ROM}	Δf_1^{REM}
a	-0.061	-0.034	-0.067					-0.046	-0.032
b	-0.021	-0.094	0.028	0.059	-0.113			-0.020	-0.006
c	-0.010	-0.098	0.029	-0.003	0.002	0.064	-0.121	-0.013	-0.002
d	-0.047	-0.033	-0.048					-0.039	-0.025
e	-0.017	-0.087	0.024	0.053	-0.089			-0.018	-0.005
f	-0.009	-0.091	0.026	-0.001	-0.000	0.059	-0.099	-0.012	-0.001
g	-0.023	-0.096	0.030	0.068	-0.134			-0.019	-0.006
h	-0.011	-0.099	0.034	-0.006	-0.001	0.075	-0.141	-0.013	-0.002
i	-0.020	-0.090	0.026	0.064	-0.112			-0.018	-0.005
j	-0.010	-0.095	0.032	-0.004	-0.003	0.072	-0.123	-0.012	-0.001

highlight the need to reduce the ROM masses to obtain good agreement in the first natural frequency. The greatest difference is observed in low-rise buildings with light floors, i.e. case a, where the fundamental frequency of ROM is 6 % lower than REM. As presumable, this error becomes smaller the higher the number of stories. For mid- and high-rise cases, with low or heavy floors, the underestimate is bounded below the 3 %.

The mass identification procedure points out that the greatest change occurs systematically on the top floor where, in several cases (b,c,g-j), the floor mass undergoes reductions greater than 10 %. Nonetheless, the variation of the total mass remains quite limited, ranging from 1 % to 5 %. In case a, a reduction of just 5 % of the total mass allows halving the error committed in frequency.

4.1 | Rigid nodes

It should be clarified that the EFM modeling approach assumes that specific portions of the masonry walls are undeformable. These portions, called *rigid nodes*, are located between two subsequent masonry piers. This assumption is legitimate in the framework in which this modeling approach has been developed, the seismic analysis of existing masonry structures. In the strongly nonlinear regime, the deformations observed for these masonry portions in buildings damaged by earthquakes are negligible compared with those of piers and spandrels, where most of the damage concentrates[62,63]. However, this simplification becomes much stronger under operational conditions – small deformation and low vibration amplitudes – and necessitates further analyses.

Rigid nodes reduce the deformable length of the pier L_s by an amount equal to the height of the rigid node L_r. According to the literature, this can be defined based on geometrical or mechanical rules[38]. The effective deformable length is, therefore, $L_{s,\text{eff}} = L_s - L_r$ and the ratio $\iota = L_{s,\text{eff}}/L_s$ expresses the deformable part of the interstory (Figure 7). A ratio equal to unity corresponds to no rigid node, as assumed in the cases already analyzed. In actual EFM of masonry buildings, on the other hand, this ratio may vary from 0.8 for a regular arrangement of openings down to 0.6 for an irregular one[38,64].

Table 6 presents the results for cases a and b introduced in the previous Section, assuming different heights of the rigid node portion. It is evident how the effect of the rigid node on the fundamental frequency is not only competing with the one caused by mass lumping but prevails over it. The introduction of rigid nodes effectively increases the stiffness of the model so that, as expected, the fundamental frequency grows rapidly as well. In particular, EFM with rigid nodes tends to overestimate the first frequency of REM. This effect is more relevant for mid-rise buildings (case b), where the number of rigid nodes increases with the number of stories.

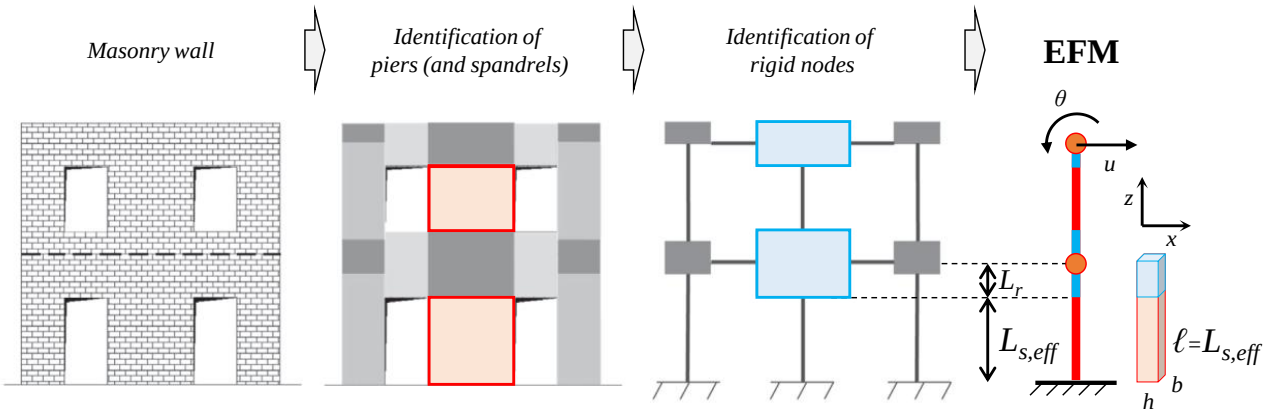

FIGURE 7 EFM of a masonry wall with rigid nodes.

TABLE 6 Mass identification for example cases a,b of Table 5, with different values of the ratio ι which represents the deformable height of the pier excluding the rigid node. The procedure adopts a first-mode oriented diagonalization (row-sum lumping method, Section 3.3).

	ROM		ROM*					
Case	ι	Δf_1^{REM}	$\Delta M_{11}^{\text{ROM}}$	$\Delta M_{22}^{\text{ROM}}$	$\Delta M_{33}^{\text{ROM}}$	$\Delta M_{44}^{\text{ROM}}$	$\Delta M_{\text{tot}}^{\text{ROM}}$	Δf_1^{REM}
	0.8	0.027	0.058	0.140			0.088	-0.031
a	0.7	0.078	0.106	0.271			0.166	-0.030
	0.6	0.133	0.156	0.423			0.253	-0.030
	0.8	0.107	-0.074	0.187	0.235	0.225	0.133	0.002
b	0.7	0.194	-0.088	0.266	0.336	0.519	0.227	0.005
	0.6	0.296	-0.121	0.346	0.447	0.915	0.334	0.008

For case a, differences in frequencies range from around 3 % for $\iota = 0.8$ and grow larger than 10 % when $\iota = 0.6$. The relative differences between the identified and starting masses are positive, meaning that floor masses should be increased. The total mass variation ranges, for case a, from around 9 % up to 25 %.

5 | CONCLUSIONS

A consistent methodological strategy has been conceived and developed to identify a low-order physics-based model with lumped mass and stiffness parameters (ROM), required to be (i) sufficiently synthetic for high-performance applications, like parametric design, state feedback controls, fast model updating, rapid health monitoring, and also (ii) sufficiently accurate to preserve the descriptive accuracy of large-sized high-fidelity models with distributed parameters (REMs), considered as ideal reference representations of a physical system under investigation.

The rationale behind the identification methodology consists of – first – searching for the desired dimension reduction of the ROM by selecting a limited configurational set of representative degrees of freedom contributing significantly to the dynamic response (spatial subsampling), while – second – pursuing the highest possible representativeness by imposing the exact coincidence of the modal properties with a selectable subset of natural frequencies and modes known from the REM (mode selection). From the mathematical viewpoint, this leading idea has been substantiated by stating an inverse indeterminate eigenproblem. By leveraging theorems of linear algebra for the existence of closed-form solutions, the inverse eigenproblem has been solved

analytically and parametrically, since its natural indeterminacy can be by-passed by selecting the lumped mass matrix as the primary unknown, and the stiffness matrix as the assigned parameter to span a family of isospectral solutions.

A comprehensive parametric analysis has been conducted by considering a multi-story frame building as a benchmark. Specifically, a high-fidelity finite element model (FEM) has been adopted as REM, while a simplified equivalent frame model (EFM) has been chosen to play the role of ROM. Before mass matrix identification, modal results have highlighted how the ROM consistently underestimates the natural frequencies of the REM. This discrepancy grows larger the lower the ratio between the floor mass and the interstory mass and is more pronounced for low-rise structures. After the mass matrix identification, the isospectral ROM is capable of completely removing the modal mismatch in terms of both frequencies and modes. The identified mass matrix is generally banded, giving rise to internal couplings of inertial nature. Therefore, different diagonalization techniques have been explored to decouple the system a posteriori, focusing on those that improve frequency agreement between fundamental modes.

To verify the proposed identification strategy for practical application to highly massive structures, a technically significant cross-section of prototypical masonry buildings has been selected and analyzed according to the EFM description. The results of the analysis reveal that low-rise masonry structures with light floors are the most affected by mass lumping. The identification procedure has suggested that reducing the model masses, particularly at the top story, may be crucial to mitigate the underestimation of the fundamental frequency. However, the impact of such an assumption on the estimate of inertial effects induced by seismic actions (i.e. the field in which, nowadays, such models are mostly diffused) must be investigated further. On the contrary, the presence of rigid nodes has a competing effect that becomes dominant in high-rise buildings and calls for additional study. The close-future developments will explore the possibility of using mass-calibrated EFM models in different lines of research, including structural health monitoring. In this context, achieving a well-balanced compromise between computational efficiency and simulation accuracy is the key to successfully fusing the virtual models with real-time streams of digital data, finally improving the traditional data-based assessment methodologies. With a look towards longer-term perspectives, the proposed methodology appears a promising candidate for emerging applications in artificial intelligence, such as dimensionality reduction in tackling high-dimensional problems and managing big data, physics-based training of neural networks, physics-informed machine learning to solve complex forward and inverse problems.

AUTHOR CONTRIBUTIONS

Daniele Sivori & **Marco Lepidi**: Conceptualization, Data curation, Formal analysis, Methodology, Software, Supervision, Validation, Visualization, Writing - original draft, Writing - review & editing. **Serena Cattari**: Conceptualization, Data curation, Formal analysis, Funding acquisition, Methodology, Software, Supervision, Validation, Visualization, Writing - original draft, Writing - review & editing.

ACKNOWLEDGMENTS

The authors thankfully acknowledge the financial support of the Italian Ministry of Education, University, and Research (MIUR) within the PRIN 2017 project DETECT-AGING – "Degradation Effects on sTructural safEty of Cultural Heritage Constructions through simulation and health monitorING" (Call 2017 — Protocol No. 201747Y73L).

FINANCIAL DISCLOSURE

None reported.

CONFLICT OF INTEREST

The authors declare no potential conflict of interest.

REFERENCES

1. Malekloo A, Ozer E, AlHamaydeh M, Girolami M. Machine learning and structural health monitoring overview with emerging technology and high-dimensional data source highlights. *Structural Health Monitoring.* 2022;21(4):1906 – 1955. doi: 10.1177/14759217211036880
2. Mishra M, Lourenço PB, Ramana G. Structural health monitoring of civil engineering structures by using the internet of things: A review. *Journal of Building Engineering.* 2022;48. doi: 10.1016/j.jobe.2021.103954
3. Dolce M, Nicoletti M, De Sortis A, Marchesini S, Spina D, Talanas F. Osservatorio sismico delle strutture: the Italian structural seismic monitoring network. *Bulletin of Earthquake Engineering.* 2017;15(2):621 – 641. doi: 10.1007/s10518-015-9738-x
4. D'Alessandro A, Costanzo A, Ladina C, et al. Urban Seismic Networks, Structural Health and Cultural Heritage Monitoring: The National Earthquakes Observatory (INGV, Italy) Experience. *Frontiers in Built Environment.* 2019;5. doi: 10.3389/fbuil.2019.00127
5. Buffarini G, Clemente P, Giovinazzi S, Ormando C, Pollino M, Rosato V. Preventing and Managing Risks Induced by Natural Hazards to Critical Infrastructures. *Infrastructures.* 2022;7(6). doi: 10.3390/infrastructures7060076
6. Di Re P, Lofrano E, Ciambella J, Romeo F. Structural analysis and health monitoring of twentieth-century cultural heritage: The Flaminio Stadium in Rome. *Smart Structures and Systems.* 2021;27(2):285 – 303. doi: 10.12989/sss.2021.27.2.285

7. Bado MF, Tonelli D, Poli F, Zonta D, Casas JR. Digital Twin for Civil Engineering Systems: An Exploratory Review for Distributed Sensing Updating. *Sensors.* 2022;22(9). doi: 10.3390/s22093168
8. Gattulli V, Franchi F, Graziosi F, et al. Design and evaluation of 5G-based architecture supporting data-driven digital twins updating and matching in seismic monitoring. *Bulletin of Earthquake Engineering.* 2022;20(9):4345–4365. doi: 10.1007/s10518-022-01329-8
9. Zhang C, Mousavi AA, Masri SF, Gholipour G, Yan K, Li X. Vibration feature extraction using signal processing techniques for structural health monitoring: A review. *Mechanical Systems and Signal Processing.* 2022;177:109175. doi: 10.1016/j.ymssp.2022.109175
10. Degli Abbati S, Sivori D, Cattari S, Lagomarsino S. Ambient vibrations-supported seismic assessment of the Saint Lawrence Cathedral's bell tower in Genoa, Italy. *Journal of Civil Structural Health Monitoring.* 2023. doi: 10.1007/s13349-023-00709-1
11. Ritto T, Rochinha F. Digital twin, physics-based model, and machine learning applied to damage detection in structures. *Mechanical Systems and Signal Processing.* 2021;155. doi: 10.1016/j.ymssp.2021.107614
12. Gattulli V, Ottaviano E, Pelliccio A. Mechatronics in the process of cultural heritage and civil infrastructure management. *Mechatronics for Cultural Heritage and Civil Engineering.* 2018:1–31. doi: 10.1007/978-3-319-68646-2_1
13. Acunzo G, Fiorini N, Mori F, Spina D. Modal mass estimation from ambient vibrations measurement: A method for civil buildings. *Mechanical Systems and Signal Processing.* 2018;98:580 – 593. doi: 10.1016/j.ymssp.2017.05.014
14. Astorga A, Guéguen P, Ghimire S, Kashima T. NDE1.0: a new database of earthquake data recordings from buildings for engineering applications. *Bulletin of Earthquake Engineering.* 2020;18(4):1321 – 1344. doi: 10.1007/s10518-019-00746-6
15. Di Girolamo GD, Smarra F, Gattulli V, Potenza F, Graziosi F, D'Innocenzo A. Data-driven optimal predictive control of seismic induced vibrations in frame structures. *Structural Control and Health Monitoring.* 2020;27(4):e2514. doi: 10.1002/stc.2514
16. Giordano PF, Iacovino C, Quqa S, Limongelli MP. The value of seismic structural health monitoring for post-earthquake building evacuation. *Bulletin of Earthquake Engineering.* 2022;20(9):4367 – 4393. doi: 10.1007/s10518-022-01375-2
17. Sivori D, Cattari S, Lepidi M. A methodological framework to relate the earthquake-induced frequency reduction to structural damage in masonry buildings. *Bulletin of Earthquake Engineering.* 2022;20(9):4603–4638. doi: 10.1007/s10518-022-01345-8
18. Vitale G, D'alessandro A, Di Benedetto A, et al. Urban Seismic Network Based on MEMS Sensors: The Experience of the Seismic Observatory in Camerino (Marche, Italy). *Sensors.* 2022;22(12). doi: 10.3390/s22124335
19. Benner P, Gugercin S, Willcox K. A survey of projection-based model reduction methods for parametric dynamical systems. *SIAM Review.* 2015;57(4):483 – 531. doi: 10.1137/130932715
20. García-Macías E, Ierimonti L, Venanzi I, Ubertini F. An Innovative Methodology for Online Surrogate-Based Model Updating of Historic Buildings Using Monitoring Data. *International Journal of Architectural Heritage.* 2021;15(1):92 – 112. doi: 10.1080/15583058.2019.1668495
21. Jaishi B, Ren WX. Structural finite element model updating using ambient vibration test results. *Journal of Structural Engineering.* 2005;131(4):617 – 628. doi: 10.1061/(ASCE)0733-9445(2005)131:4(617)
22. Cattari S, Sivori D, Alfano S, et al. Calibration of numerical models to support SHM: The consoli palace of Gubbio, Italy. In: *Proceedings of the 8th International Conference on Computational Methods in Structural Dynamics and Earthquake Engineering Methods in Structural Dynamics and Earthquake Engineering (COMPDYN 2021)* 2021; Streamed from Athens, Greece, 28–30 June:3778 - 3794
23. Standoli G, Salachoris GP, Masciotta MG, Clementi F. Modal-based FE model updating via genetic algorithms: Exploiting artificial intelligence to build realistic numerical models of historical structures. *Construction and Building Materials.* 2021;303. doi: 10.1016/j.conbuildmat.2021.124393
24. Salachoris GP, Standoli G, Betti M, Milani G, Clementi F. Evolutionary numerical model for cultural heritage structures via genetic algorithms: a case study in central Italy. *Bulletin of Earthquake Engineering.* 2023. doi: 10.1007/s10518-023-01615-z
25. Lagomarsino S, Penna A, Galasco A, Cattari S. TREMURI program: An equivalent frame model for the nonlinear seismic analysis of masonry buildings. *Engineering Structures.* 2013;56:1787 – 1799. doi: 10.1016/j.engstruct.2013.08.002
26. Quagliarini E, Maracchini G, Clementi F. Uses and limits of the Equivalent Frame Model on existing unreinforced masonry buildings for assessing their seismic risk: A review. *Journal of Building Engineering.* 2017;10:166 – 182. doi: 10.1016/j.jobe.2017.03.004
27. Cattari S, Calderoni B, Caliò I, et al. Nonlinear modeling of the seismic response of masonry structures: critical review and open issues towards engineering practice. *Bulletin of Earthquake Engineering.* 2022;20(4):1939 – 1997. doi: 10.1007/s10518-021-01263-1
28. Manzini CF, Morandi P, Magenes G. SAM-II: development and validation of an EF-based program for seismic pushover analysis of masonry buildings. *Bulletin of Earthquake Engineering.* 2023;21(14):6317 – 6365. doi: 10.1007/s10518-023-01767-y
29. Cattari S, Camilletti D, D'Altri AM, Lagomarsino S. On the use of continuum Finite Element and Equivalent Frame models for the seismic assessment of masonry walls. *Journal of Building Engineering.* 2021;43. doi: 10.1016/j.jobe.2021.102519
30. Sivori D, Ierimonti L, Venanzi I, Ubertini F, Cattari S. An Equivalent Frame Digital Twin for the Seismic Monitoring of Historic Structures: A Case Study on the Consoli Palace in Gubbio, Italy. *Buildings.* 2023;13(7). doi: 10.3390/buildings13071840
31. Sivori D, Lepidi M, Cattari S. Structural identification of the dynamic behavior of floor diaphragms in existing buildings. *Smart Structures and Systems.* 2021;27(2):173 – 191. doi: 10.12989/sss.2021.27.2.173
32. Cattari S, Alfano S, Lagomarsino S. A Practice-Oriented Proposal to Consider the Flange Effect in Equivalent Frame Modeling of Masonry Buildings. *Buildings.* 2023;13(2). doi: 10.3390/buildings13020462
33. Karniadakis GE, Kevrekidis IG, Lu L, Perdikaris P, Wang S, Yang L. Physics-informed machine learning. *Nature Reviews Physics.* 2021;3(6):422 – 440. doi: 10.1038/s42254-021-00314-5
34. Vrtač T, Ocepek D, Česnik M, Čepon G, Boltežar M. A hybrid modeling strategy for training data generation in machine learning-based structural health monitoring. *Mechanical Systems and Signal Processing.* 2024;207. doi: 10.1016/j.ymssp.2023.110937
35. Whiteman ML, Marin-Artieda CC, Tezcan J. Convolutional Neural Network Approach for Vibration-Based Damage State Prediction in a Reinforced Concrete Building. *Journal of Computing in Civil Engineering.* 2024;38(2). doi: 10.1061/JCCEE5.CPENG-5511
36. Cattari S, Degli Abbati S, Alfano S, Brunelli A, Lorenzoni F, Porto dF. Dynamic calibration and seismic validation of numerical models of URM buildings through permanent monitoring data. *Earthquake Engineering and Structural Dynamics.* 2021;50(10):2690 – 2711. doi: 10.1002/eqe.3467
37. Parisi F, Augenti N. Seismic capacity of irregular unreinforced masonry walls with openings. *Earthquake Engineering and Structural Dynamics.* 2013;42(1):101 – 121. doi: 10.1002/eqe.2195
38. Cattari S, D'Altri AM, Camilletti D, Lagomarsino S. Equivalent frame idealization of walls with irregular openings in masonry buildings. *Engineering Structures.* 2022;256. doi: 10.1016/j.engstruct.2022.114055

39. Costa C, Arêde A, Costa A, Caetano E, Cunha A, Magalhaes F. Updating Numerical Models of Masonry Arch Bridges by Operational Modal Analysis. *International Journal of Architectural Heritage.* 2015;9(7):760 – 774. doi: 10.1080/15583058.2013.850557
40. Standoli G, Giordano E, Milani G, Clementi F. Model Updating of Historical Belfries Based on Oma Identification Techniques. *International Journal of Architectural Heritage.* 2021;15(1):132 – 156. doi: 10.1080/15583058.2020.1723735
41. Friswell MI. Damage identification using inverse methods. *Philosophical Transactions of the Royal Society A: Mathematical, Physical and Engineering Sciences.* 2007;365(1851):393 – 410. doi: 10.1098/rsta.2006.1930
42. Peeters B, Roeck GD. Stochastic system identification for operational modal analysis: A Review. *Journal of Dynamic Systems, Measurement and Control, Transactions of the ASME.* 2001;123(4):659 – 667. doi: 10.1115/1.1410370
43. Rainieri C, Fabbrocino G. Automated output-only dynamic identification of civil engineering structures. *Mechanical Systems and Signal Processing.* 2010;24(3):678 – 695. doi: 10.1016/j.ymssp.2009.10.003
44. Reynders E. System Identification Methods for (Operational) Modal Analysis: Review and Comparison. *Archives of Computational Methods in Engineering.* 2012;19(1):51 – 124. doi: 10.1007/s11831-012-9069-x
45. Sadhu A, Narasimhan S, Antoni J. A review of output-only structural mode identification literature employing blind source separation methods. *Mechanical Systems and Signal Processing.* 2017;94:415 – 431. doi: 10.1016/j.ymssp.2017.03.001
46. Hoshiya M, Saito E. Structural identification by extended Kalman filter. *Journal of Engineering Mechanics.* 1984;110(12):1757 – 1770. doi: 10.1061/(ASCE)0733-9399(1984)110:12(1757)
47. Roemer M, Monk D. Mass, stiffness, and damping matrix identification: An integrated approach. *Journal of Vibration and Acoustics, Transactions of the ASME.* 1992;114(3):358 – 363. doi: 10.1115/1.2930270
48. Yang JN, Lei Y, Pan S, Huang N. System identification of linear structures based on Hilbert-Huang spectral analysis. Part 1: Normal modes. *Earthquake Engineering and Structural Dynamics.* 2003;32(9):1443 – 1467. doi: 10.1002/eqe.287
49. Yang JN, Lei Y, Pan S, Huang N. System identification of linear structures based on Hilbert-Huang spectral analysis. Part 2: Complex modes. *Earthquake Engineering and Structural Dynamics.* 2003;32(10):1533 – 1554. doi: 10.1002/eqe.288
50. Doebling SW, Farrar CR. Computation of structural flexibility for bridge health monitoring using ambient modal data. In: *Proceedings of the 11th ASCE Engineering Mechanics Conference*. 2. 1996; Fort Lauderdale, FL, USA, 20–-22 May:1114 – 1117.
51. Parloo E, Verboven P, Guillaume P, Van Overmeire M. Sensitivity-based operational mode shape normalisation. *Mechanical Systems and Signal Processing.* 2002;16(5):757 – 767. doi: 10.1006/mssp.2002.1498
52. Thoren A. Derivation of mass and stiffness matrices from dynamic test data. In: *Proceedings of the 13th Structures, Structural Dynamics, and Materials Conference* 1972; San Antonio, TX, U.S.A., 10–12 April:346
53. Baruch M. Modal data are insufficient for identification of both mass and stiffness matrices. *AIAA Journal.* 1997;35(11):1797 – 1798. doi: 10.2514/2.36
54. Khatri CG, Mitra SK. Hermitian and Nonnegative Definite Solutions of Linear Matrix Equations. *SIAM Journal on Applied Mathematics.* 1976;31(4):579-585. doi: 10.1137/0131050
55. Baksalary JK. Nonnegative Definite and Positive Definite Solutions to the Matrix Equation $AXA^* = B$. *Linear and Multilinear Algebra.* 1984;16(1-4):133 – 139. doi: 10.1080/03081088408817616
56. Groß J. Nonnegative-definite and positive-definite solutions to the matrix equation $AXA^* = B$ - Revisited. *Linear Algebra and Its Applications.* 2000;321(1-3):123 – 129. doi: 10.1016/S0024-3795(00)00033-1
57. Lepidi M. Multi-parameter perturbation methods for the eigensolution sensitivity analysis of nearly-resonant non-defective multi-degree-of-freedom systems. *Journal of Sound and Vibration.* 2013;332(4):1011–1032. doi: 10.1016/j.jsv.2012.09.020
58. Gladwell G. Isospectral Vibrating Systems. *Advances in Engineering Structures, Mechanics & Construction.* 2006:31–38.
59. Sivori D, Lepidi M, Cattari S. Isospectral stiffness matrix identification for the Equivalent Frame modeling of buildings. In: *Proceedings of the 10th International Operational Modal Analysis Conference (IOMAC 2024)* 2024; Naples, Italy, 21–24 May. Accepted.
60. Allemang RJ. The modal assurance criterion - Twenty years of use and abuse. *Sound and Vibration.* 2003;37(8):14 – 21.
61. Sivori D, Lepidi M, Cattari S. Ambient vibration tools to validate the rigid diaphragm assumption in the seismic assessment of buildings. *Earthquake Engineering and Structural Dynamics.* 2020;49(2):194 – 211. doi: 10.1002/eqe.3235
62. Penna A, Morandi P, Rota M, Manzini CF, Porto dF, Magenes G. Performance of masonry buildings during the Emilia 2012 earthquake. *Bulletin of Earthquake Engineering.* 2014;12(5):2255 – 2273. doi: 10.1007/s10518-013-9496-6
63. Sorrentino L, Cattari S, Porto dF, Magenes G, Penna A. Seismic behaviour of ordinary masonry buildings during the 2016 central Italy earthquakes. *Bulletin of Earthquake Engineering.* 2019;17(10):5583 – 5607. doi: 10.1007/s10518-018-0370-4
64. Ottonelli D, Manzini CF, Marano C, Cordasco EA, Cattari S. A comparative study on a complex URM building: part I—sensitivity of the seismic response to different modelling options in the equivalent frame models. *Bulletin of Earthquake Engineering.* 2022;20(4):2115 – 2158. doi: 10.1007/s10518-021-01128-7
65. Felippa CA. Construction of customized mass-stiffness pairs using templates. *Journal of Aerospace Engineering.* 2006;19(4):241 – 258. doi: 10.1061/(ASCE)0893-1321(2006)19:4(241)
66. Felippa CA, Guo Q, Park K. Mass Matrix Templates: General Description and 1D Examples. *Archives of Computational Methods in Engineering.* 2015;22(1):1 – 65. doi: 10.1007/s11831-014-9108-x
67. Stewart G. On the Sensitivity of the Eigenvalue Problem $Ax = \lambda Bx$. *SIAM Journal on Numerical Analysis.* 1972;9(4):669 – 686. doi: 10.1137/0709056
68. Guyan RJ. Reduction of stiffness and mass matrices. *AIAA Journal.* 1965;3(2):380. doi: 10.2514/3.2874
69. Irons B. Structural eigenvalue problems - elimination of unwanted variables. *AIAA Journal.* 1965;3(5):961 – 962. doi: 10.2514/3.3027

□

APPENDIX

A INVERSE SPECTRAL EIGENPROBLEM: MASS MATRIX IDENTIFICATION

Independently of its completeness, the data $\mathbf{K}, \mathbf{M}$ and the solution $\mathbf{\Lambda}, \mathbf{\Phi}$ of the direct eigenproblem (Section 2.1, Eq. (1)) satisfies the matrix relationship

$$\mathbf{K}\mathbf{\Phi} = \mathbf{M}\mathbf{\Phi}\mathbf{\Lambda} \tag{A1}$$

which can be transposed to read

$$\mathbf{\Phi}^\top\mathbf{K}^\top = \mathbf{\Lambda}^\top\mathbf{\Phi}^\top\mathbf{M}^\top \tag{A2}$$

where the properties of transposition have been employed. Therefore, the symmetry properties $\mathbf{K}^\top = \mathbf{K}$ and $\mathbf{M}^\top = \mathbf{M}$ (by hypothesis) and $\mathbf{\Lambda}^\top = \mathbf{\Lambda}$ (by construction) allows to rewrite

$$\mathbf{\Lambda}\mathbf{\Phi}^\top\mathbf{M} = \mathbf{\Phi}^\top\mathbf{K} \tag{A3}$$

which can be regarded, by inverting the role of data $\mathbf{\Lambda}, \mathbf{\Phi}$ and unknown $\mathbf{K}, \mathbf{M}$, as an inverse eigenproblem.

The inverse eigenproblem can be solved by recognizing that (A3) represents, for the unknown matrix $\mathbf{M}$ (Section 2.2), a linear matrix equation of the form

$$\mathbf{A}\mathbf{X} = \mathbf{C} \tag{A4}$$

having made the positions $\mathbf{A} = \mathbf{\Lambda}\mathbf{\Phi}^\top \in \mathbb{R}^{M\times N} \subset \mathbb{C}^{M\times N}$ and $\mathbf{C} = \mathbf{\Phi}^\top\mathbf{K} \in \mathbb{R}^{M\times N} \subset \mathbb{C}^{M\times N}$. According to Theorems of Linear Algebra[54], the solution $\mathbf{X}$ exists and is Hermitian, that is $\mathbf{X}^* = \mathbf{X}$, if and only if

$$\mathbf{C}\mathbf{A}^* = \mathbf{C}\mathbf{A}^\top \quad \textit{is Hermitian} \tag{A5}$$

that is, by inverting the positions and replacing $\mathbf{X}$ with $\mathbf{M}$, the unknown mass matrix $\mathbf{M}$ is Hermitian if and only if

$$\begin{aligned}\mathbf{\Phi}^\top\mathbf{K}\left(\mathbf{\Lambda}\mathbf{\Phi}^\top\right)^* &= \mathbf{\Phi}^\top\mathbf{K}\left(\mathbf{\Lambda}\mathbf{\Phi}^\top\right)^\top \qquad \text{being } \mathbf{\Lambda}\in\mathbb{R}^{M\times M}, \mathbf{\Phi}\in\mathbb{R}^{N\times M}\\ &= \mathbf{\Phi}^\top\mathbf{K}\mathbf{\Phi}\mathbf{\Lambda}^\top\\ &= \mathbf{\Phi}^\top\mathbf{K}\mathbf{\Phi}\mathbf{\Lambda} \quad \textit{is Hermitian}\end{aligned} \tag{A6}$$

which is certainly satisfied given the orthonormality of the eigenvectors $\boldsymbol{\phi}_i$ with respect the stiffness matrix $\mathbf{K}$, i.e. $\boldsymbol{\phi}_i^\top\mathbf{K}\boldsymbol{\phi}_j = \delta_{ij}$. If the condition (A5) is satisfied, the Hermitian solution of Eq. (A3) has general expression

$$\mathbf{X} = \mathbf{A}^\dagger\mathbf{C} + \mathbf{C}^*\left(\mathbf{A}^\dagger\right)^* - \mathbf{A}^\dagger\mathbf{A}\mathbf{C}^*\left(\mathbf{A}^\dagger\right)^* + \left[\mathbf{I} - \mathbf{A}^\dagger\mathbf{A}\right]\mathbf{Z}\left[\mathbf{I} - \mathbf{A}^\dagger\mathbf{A}\right]^* \tag{A7}$$

where $\mathbf{I}\in\mathbb{R}^{N\times N}$ is the identity matrix and $\mathbf{Z}\in\mathbb{C}^{N\times N}$ is an arbitrary Hermitian matrix. By inverting the positions and replacing $\mathbf{X}$ with $\mathbf{M}$, the solution (2) is achieved.

B TIMOSHENKO PLANE BEAM ELEMENT

The Timoshenko plane beam element adopted in this work (Section 3) is characterized by two end nodes and four nodal displacements, collected in the column vector $\boldsymbol{u}^e = (u_1, \theta_1, u_2, \theta_2)$. The stiffness matrix of the finite element is

$$\mathbf{K}^e = \frac{EI}{\ell^3(1+\Psi)}\begin{bmatrix} 12 & 6\ell & -12 & 6\ell \\ 6\ell & \ell^2(4+\Psi) & -6\ell & \ell^2(2-\Psi) \\ -12 & -6\ell & 12 & -6\ell \\ 6\ell & \ell^2(2-\Psi) & -6\ell & \ell^2(4+\Psi) \end{bmatrix}, \quad \Psi = \frac{12EI}{GA_s\ell^2} \tag{B8}$$

where E is the elastic Young modulus of the material, I is the second moment of the cross-section area, ℓ is the element length and Ψ is an adimensional coefficient characterizing the beam shear slenderness – depending, among the others, on the shear modulus $G = E/(2(1+\nu))$, where ν is the Poisson coefficient, and shear area $A_s = \kappa A = \kappa bh$, where κ is the Timoshenko

coefficient. Such a matrix is optimal (i.e. nodally exact) for the static analysis of a prismatic beam member. For a rectangular cross-section, I and κ take the well known expressions

$$I = \frac{bh^3}{12}, \quad \kappa = \frac{10(1+\nu)}{12+11\nu}.$$

The mass matrix of the finite element is assumed to be diagonally lumped (Diagonal Lumped Mass Matrix, DLMM[65,66]) with zero mass assigned to the rotational degrees of freedom. The matrix takes the form

$$\mathbf{M}^e = \rho A \ell \begin{bmatrix} 1/2 & 0 & 0 & 0 \\ 0 & 0 & 0 & 0 \\ 0 & 0 & 1/2 & 0 \\ 0 & 0 & 0 & 0 \end{bmatrix} \tag{B9}$$

which satisfies the conservation of linear momentum (but not angular momentum). This choice, often referred to as *inconsistent*, makes $\mathbf{M}^e$ a singular, symmetric positive semi-definite matrix.

C STATIC CONDENSATION

Due to the singular form of the element mass matrix $\mathbf{M}^e$ (see Appendix B), the direct eigenproblem for matrix $\mathbf{K} \in \mathbb{R}^{N\times N}$ with respect to the matrix $\mathbf{M} \in \mathbb{R}^{N\times N}$ (Section 2.1) degenerates, since the characteristic polynomial $\det(\mathbf{K} - \lambda\mathbf{M})$ is of degree less than N and the problem can be said to have one or more infinite eigenvalues[67].

The inverse eigenproblem (Section 2.2) is still solvable by considering an incomplete set of modes, i.e. neglecting those modes with an infinite eigenvalue. This strategy, however, loosens the constraints of the matrix inversion and impacts negatively on the identification procedure, reducing the accuracy of the identified mass matrix.

This issue can be overcome by taking advantage of the well-known static condensation technique, also known as the Iron-Guyan's reduction scheme[68,69]. The process involves the condensation of massless nodal displacements, the rotations θ in this case, which are first expressed in terms of translations u and then omitted from the problem formulation. The quasi-static condensation, other than reducing the model order, effectively removes the singularity of the mass matrix without altering its inertial properties. The condensed eigensolution is, algorithmically, exact, with no approximation with respect to the original one.

The eigenvalue problem (Section 2.1, Eq 1) is rearranged and partitioned as

$$\begin{bmatrix} \mathbf{K}_{uu} & \mathbf{K}_{u\theta} \\ \mathbf{K}_{\theta u} & \mathbf{K}_{\theta\theta} \end{bmatrix} \begin{bmatrix} \mathbf{\Phi}_u \\ \mathbf{\Phi}_\theta \end{bmatrix} = \lambda \begin{bmatrix} \mathbf{M}_{uu} & \mathbf{O} \\ \mathbf{O} & \mathbf{O} \end{bmatrix} \begin{bmatrix} \mathbf{\Phi}_u \\ \mathbf{\Phi}_\theta \end{bmatrix} \tag{C10}$$

Solving the lower sub-equation for $\mathbf{\Phi}_\theta$ we obtain

$$\mathbf{\Phi}_\theta = -\mathbf{K}_{\theta\theta}^{-1}\mathbf{K}_{\theta u}\mathbf{\Phi}_u \tag{C11}$$

and substituting in the upper one we obtain the so-called *condensed* form of the eigenproblem

$$\mathbf{K}_u\mathbf{\Phi}_u = \lambda\mathbf{M}_{uu}\mathbf{\Phi}_u, \quad \mathbf{K}_u = \mathbf{K}_{uu} - \mathbf{K}_{u\theta}\mathbf{K}_{\theta\theta}^{-1}\mathbf{K}_{\theta u} \tag{C12}$$

whose solution provides a set of eigenvalues λ_i and associated eigentranslations $\mathbf{\Phi}_{ui}$ which correspond to the nondegenerate eigenpairs of the original problem. Condensed eigenrotations $\mathbf{\Phi}_{\theta i}$ can be directly recovered using Eq. (C11).